CHAPTER 1

Introduction

1.1 Background and motivation

This thesis presents an investigation of the accuracy of various circular flexure hinge compliance (inverse of stiffness) equations and the modelling of the kinetostatics (describes both the kinematics and statics) of micro-motion stages. Two planar mechanism topologies are studied in this thesis, which are a four-bar and a 3-RRR (revolute-revolute-revolute) compliant micro-motion stage. The two compliant micro-motion stages and their topological diagrams are shown in Figure 1.1. A prototype of the 3-RRR micro-motion stage is shown in Figure 1.2. This prototype was used to conduct experiments to verify analytical and FEA models. The four-bar compliant mechanism has one-degree-of-freedom (DOF) and it consists of four circular flexure hinges. The 3-RRR compliant micro-motion stage has three-DOF, which are the translational motions in the x- and y-axis and the rotational motions about the z-axis. It consists of three RRR links arranged in parallel and each link has three circular flexure hinges. The 3-RRR compliant stage was designed to be used in a scanning-electron-microscope (SEM). The design specifications of the stage can be found in Handley (2006).

The kinetostatic model of a simple mechanism, in this case the four-bar mechanism, was derived initially. The methodology of deriving the kinetostatic model was then extended to a more complicated topology, which was the 3-RRR compliant micro-motion stage. The purpose of presenting the derivation of the kinetostatic models of these two compliant mechanisms is to demonstrate that the methodology is applicable to different topologies of planar compliant mechanisms.

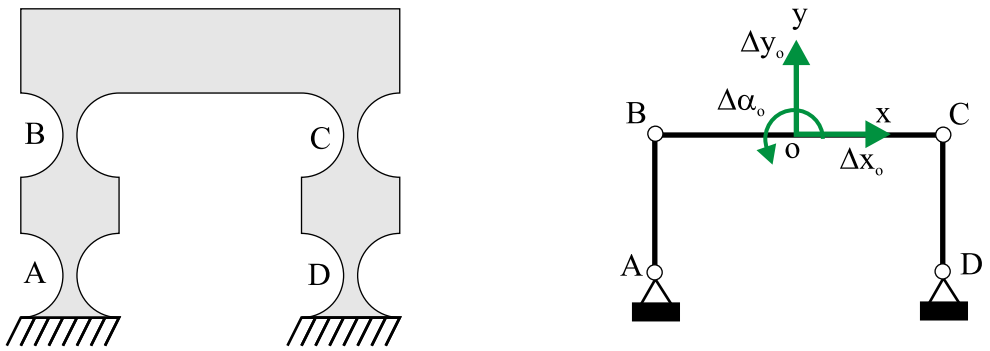

(a) Four-bar micro-motion stage

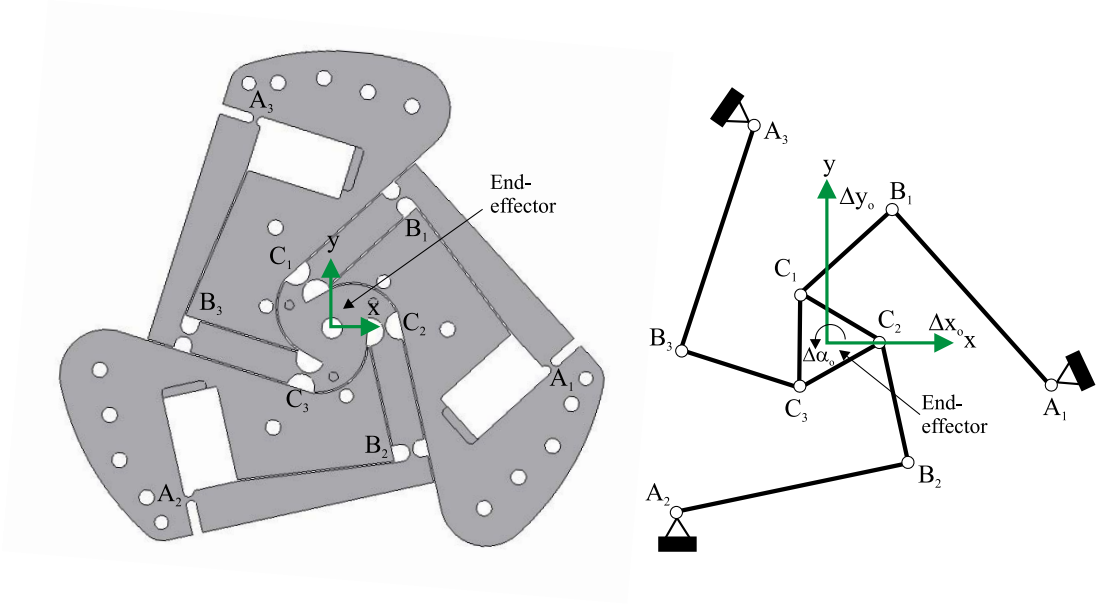

(b) 3-RRR micro-motion stage

Figure 1.1: Compliant micro-motion stages and their topological diagrams

Nevertheless, the main focus of this thesis is the 3-RRR compliant micro-motion stage.

Micro-motion stages have emerged as an important technological advancement in the past three decades. The significance of this advancement is highlighted in many applications where the positioning of components with accuracies in the micrometre or nanometre range is required. Examples include the positioning of samples in a scanning-electron-microscopes (SEM), the alignment of fibre-optics and lasers, the positioning of masks in lithography, the manipulation of cells in micro-biology and the manipulation of micro-scale components in micro-assembly.

Most of the micro-motion stages are designed based on the compliant mechanism concept. Compliant mechanisms generate their motions through elastic

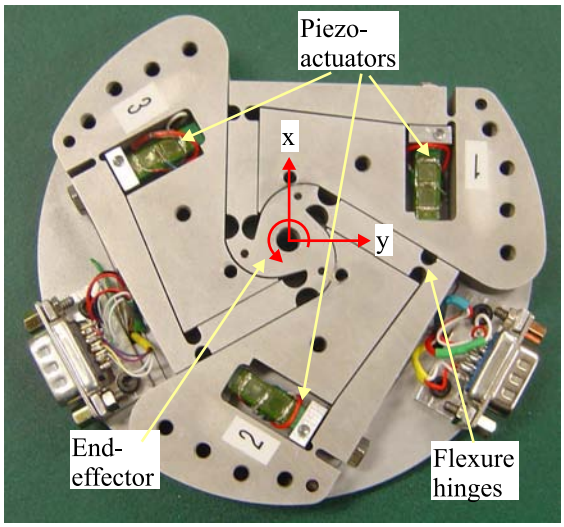

Figure 1.2: Prototype of the 3-RRR micro-motion stage

deformations. These mechanisms replace most of their joints in rigid-link mechanisms using flexure hinges. Compliant mechanisms are commonly machined from a single piece of material and no assembly of parts is required. Therefore, compliant mechanisms are advantageous over rigid-link designs where the number of parts for compliant mechanisms is reduced, resulting in weight savings. Compliant mechanisms also avoid the use of moving and sliding joints. Thus, the problem of wear, backlash, friction and need for lubrication can be eliminated.

Compliant micro-motion stages are capable of achieving sub-micrometre or even sub-nanometre positioning resolution. The positioning resolution of a micro-motion stage is only limited by the resolution of the actuators and position sensors which are used to detect the motion.

Many actuation principles have been applied to drive micro-motion stages. Piezoelectric stack actuators (hereafter referred to as piezo-actuators), electrostatic, electromagnetic and shape memory alloy actuators have been utilised to provide fine motions to micro-motion stages. Piezo-actuators are commonly used to provide fine resolution of input displacements, potentially in the sub-nanometre range depending on the noise of the voltage signal applied. Piezo-actuators were used as driving elements in the compliant micro-motion stage studied in this thesis (see Figure 1.2).

The four bar and 3-RRR micro-motion stages studied in this thesis have parallel structure configurations which are advantageous over serial structures. All actuators of parallel structures can be located at the base, thus reducing the link mass. A parallel structure also has a high mechanical stiffness, high motion accuracy and high resonant frequency. Therefore, parallel structures are better than serial

structures for applications requiring high positioning accuracy and speed. 3-RRR compliant stages also have a symmetrical configuration, and thus are less sensitive to temperature variations that could change the kinematics of the structure due to material expansion or contraction.

Despite all the advantages aforementioned, there are some disadvantages associated with compliant micro-motion stages with flexure hinges. For example, it is more complicated to model and to control the motion of compliant stages precisely compared to the well understood rigid-body mechanisms with simple revolute joints. This is partly due to the fact that flexure hinges possess more than one-DOF. Unlike revolute joints which have only the rotational motion about the z-axis, flexure hinges have both translational and rotational motions in the x-, y- and z-axis (a total of six-DOF which are Δx, Δy, Δz, $\Delta\alpha_x$,$\Delta\alpha_y$ and $\Delta\alpha_z$). All micro-motion stages studied in this thesis are planar structures and circular flexure hinges with high out-of-plane stiffnesses are used. Therefore, circular flexure hinges could be modelled to have only three in-plane DOFs, which are the translation DOFs (Δx and Δy) in the x and y axes, and the rotational DOF ($\Delta\alpha_z$) about the z-axis (see Figure 1.3). Although this assumption simplifies the modelling of circular flexure hinges, the modelling of micro-motion stages are still far more complicated than rigid-body mechanisms. There are a number of modelling methods that have been previously applied to model the kinematics (motions) and statics (stiffnesses/compliances) of micro-motion stages, however the error of some of these analytical models are large when compared to FEA and experimental results. This is partly due to the fact that flexure hinges are modelled to have only one or two-DOF. For example, the method of the Pseudo-Rigid-Body-Model (PRBM) is commonly used to predict the displacement of compliant mechanisms. The PRBM commonly models a flexure hinge as a revolute joint (one-DOF) with an attached torsional spring. The thick sections joining the flexure hinges are modelled as rigid links. The accuracy of the kinematics predicted using the PRBM reduces when the Δx- and Δy-deformations of flexure hinges are ignored. The inaccuracy of the PRBM method that excluded the modelling of the Δx- and Δy-deformations of flexure hinges was reported previously in various published research studies and will be presented in the literature review chapter.

The presence of large errors of some previously derived models of micro-motion stages could also be attributed to the inaccurate modelling of flexure hinges. Since a compliant micro-motion stage uses a few flexure hinges to provide the desired motions through deformations, the accuracy of the kinetostatic model of micro-motion stages partly relies on the accuracy of flexure hinge models. Compliance equations of flexure hinges are required to be as accurate as possible to reduce

the accumulated modelling errors from flexure hinges in a compliant structure. A great deal of research has been conducted in modelling the compliance of circular flexure hinges. However, it was not clear that these compliance equations would be suitable for application on different values of the geometrical ratio, t/R (see Figure 1.3) of circular flexure hinges. There was no proper scheme developed for selecting the most suitable flexure hinge equations (with certain t/R ratios) for hinge compliance calculations. A scheme for selecting the most suitable hinge equations for circular flexure hinges with certain t/R ratios is presented in this thesis.

Currently, published research regarding the aspects of kinetostatics of micro-motion stages is limited. The development of the kinetostatic model allows the fulfillment of both the kinematics and the statics design criteria (Krovi *et al.*, 2002) of micro-motion stages. A precise kinetostatic model of compliant micro-motion stages will benefit researchers in at least the design and optimization phases where a good estimation of kinematics, workspace or stiffness of a micro-motion stage could be realised. The kinetostatic model is also an alternative method to the finite-element approach which uses commercially available software. The modelling and meshing procedures using finite-element software is relatively time consuming and costly.

A simple methodology of deriving kinetostatic models for micro-motion stages with different topologies are presented in this thesis. The kinetostatic model is simple and has closed-form equations. These closed-form equations are expressed in terms of flexure hinge compliances, material properties and geometrical parameters. Flexure hinges in the kinetostatic model derived in this thesis are modelled to have three-DOF; therefore this kinetostatic model is expected to be more accurate than the PRBM method which excludes the modelling of the Δx- and Δy-deformations of flexure hinges. Flexure hinges in the kinetostatic model are modelled to have only three-DOF instead of all six-DOF because micro-motion stages studied in this thesis are planar stages with a large thickness b (see Figure 1.3). Therefore the out-of-plane DOFs ($\Delta\alpha_x$, $\Delta\alpha_y$ and Δz) are not taken into consideration.

1.2 Objectives and scope

This thesis only involves the study of planar micro-motion stages with circular flexure hinges. Therefore, only in-plane motions of flexure hinges and micro-motion stages are considered. Flexure hinges are modelled to have only three-DOF. Finite-element-analysis (FEA) models of flexure hinges and micro-motion stages developed in this thesis are two-dimensional models. There are two major

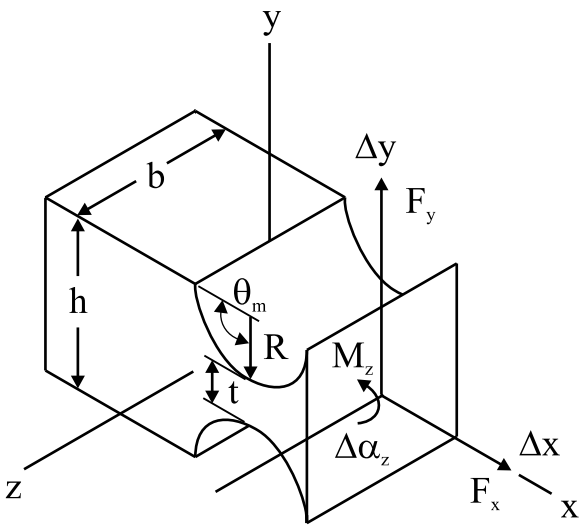

Figure 1.3: Circular flexure hinge

objectives in this thesis.

Objective 1 There are various flexure hinge equations derived previously using different methods to predict the compliances of flexure hinges. However, some of the analytical/empirical compliance equations provide better accuracies than others depending on the t/R ratio of circular flexure hinges, and flexure hinge compliance equations derived previously by any particular method may not be suitable for a large range of t/R ratios. There is no proper scheme developed up to this date on how to select the most suitable and accurate hinge equations from the previously derived equations. Therefore, the first objective of this thesis is to investigate the accuracy and limitation of previously derived compliance equations of circular flexure hinges based on their t/R ratios, and therefore to develop a scheme to guide designers for selecting the most suitable hinge equation based on the t/R ratio of flexure hinges.

Objective 2 The second objective is to develop a simple methodology of deriving an accurate kinetostatic model of compliant mechanisms by incorporating the scheme developed in Objective 1. The methodology models flexure hinges to have three in-plane DOF. The kinetostatic model is derived to have closed-form equations. Compliances of flexure hinges are one of the variables in the model. Therefore the most suitable flexure hinge equations can be selected based on the scheme developed in Objective 1 to calculate the kinetostatics of micro-motion stages accurately.

1.3 Organisation of thesis

A literature review is presented in Chapter 2. Chapter 3 presents a review on various flexure hinge equations by comparing the results of the equations with that of FEA models. A scheme for selecting the most suitable flexure hinge equations based on the t/R ratios of circular flexure hinges is then presented. Analytical kinematic modelling of compliant micro-motion stages using the PRBM method and the loop-closure theory (which excludes the modelling of the Δx- and Δy-deformations of flexure hinges) are presented in Chapter 4. The derivation of the kinetostatic model of compliant micro-motion stages are presented in Chapter 5. In Chapter 6, the FEA modelling methods of the micro-motion stages using ANSYS are presented. The results of the PRBM and the kinetostatic models are compared to the FEA results and the differences are discussed. Chapter 7 presents the experimental equipment, techniques and setup used to verify the analytical and FEA models developed in Chapter 4, 5 and 6. Results of the PRBM, the kinetostatic models and the FEA are compared with the experimental results and their differences are discussed. Conclusions and suggestions for future work are presented in Chapter 8.

CHAPTER 2

Literature Review

This chapter provides a thorough review of the literature relating to the modelling of flexure hinges and compliant micro-motion stages. An in-depth discussion of various profiles of flexure hinges and various modelling methods used to derive flexure hinge compliance equations are presented. The kinematic, static and kinetostatic modelling of various micro-motion stages are also discussed in-depth. Gaps in current knowledge are identified which provide the main aims of this study.

At this point, it may be useful to clarify some phrases used in this thesis,

- **compliance** is the inverse of stiffness;
- **compliances of flexure hinges** refer to deformations of flexure hinges due to forces/moment applied at the flexure hinges (see Figure 1.3);
- **compliances of micro-motion stages** refer to deformations of stages (which consists of several flexure hinges) when forces/moment are applied at the stage;
- **degrees-of-freedom (DOF) of flexure hinges:** It will be frequently mentioned in this thesis that flexure hinges are modelled to have certain DOFs. This indicates that flexure hinges may be modelled with translational and rotational deformations along the x, y and z axes (see Figure 1.3). These deformations are also referred to as Δx-, Δy-, Δz-, $\Delta\alpha_x$-, $\Delta\alpha_y$- and $\Delta\alpha_z$-deformations;

- **degrees-of-freedom (DOF) of micro-motion stages** refer to the DOF of the end-effector of the micro-motion stages; and

- **flexure hinge compliance equations** refer to equations derived to calculate in-plane compliances, $\Delta x/F_x$, $\Delta y/F_y$, $\Delta\alpha_z/M_z$ and out-of-plane compliances, $\Delta\alpha_x/M_x$, $\Delta\alpha_y/M_y$, $\Delta z/F_z$ of flexure hinges.

2.1 Modelling of flexure hinges

The motion range, workspace and stiffness of compliant micro-motion stages are heavily affected by the topology of the stage, and the profiles and stiffnesses of flexure hinges. Most of the flexure hinges are designed to provide rotational compliances about the z-axis. However, the compliances at other axes are unavoidable. The parameters and profiles of flexure hinges affect the compliances and motion ranges of flexure hinges. For example, the compliance of flexure hinges vary with the smallest thickness t, the radius R, the angle of the curvature θ_m, the cross-sectional thickness b (see Figure 1.3 for dimensions) and the material properties of the hinge. The accuracy of a compliant micro-motion stage model partly relies on the accuracy of the flexure hinge modelling. Therefore, compliance equations of flexure hinges are demanded to be as accurate as possible to reduce the accumulated modelling errors of hinges in a compliant stage.

This literature review of flexure hinges focuses on the modelling of hinges which display a linear elastic behaviour. Flexure hinges are classified into different profiles such as circular, leaf-spring, beam-type, elliptical, corner-filleted, parabolic and hyperbolic (Paros and Weisbord, 1965; Smith *et al.*, 1997; Lobontiu *et al.*, 2001, 2002a). In early designs, circular flexure hinges were widely used due to the ease of machining of these profiles. Circular hinges could be easily manufactured by drilling two closely spaced holes on a flat piece of material. Therefore, compliances of circular flexure hinges have been studied intensively (Paros and Weisbord, 1965; Smith *et al.*, 1987; Her and Chang, 1994; Xu and Qu, 1996; Zhang and Fasse, 2001; Tseytlin, 2002; Wu and Zhou, 2002; Lobontiu, 2003). In recent years, the advancement of manufacturing techniques, in particular wire-electrical-discharge-machining (wire-EDM) has made the accurate manufacturing of the leaf-spring, elliptical, corner-filleted, parabolic and hyperbolic flexure hinge profiles possible.

Paros and Weisbord (1965) were the first group to introduce circular flexure hinges. They formulated the design equations, including both the full and simplified equations, to calculate compliances of circular flexure hinges in the x, y

and z axes. Their simplified equations must satisfy two assumptions, which are $t/2R \ll 1$ and $t/2R \ll h/2R$, in order to obtain accurate compliance results of flexure hinges. The differences of their simplified equations relative to their full equations were within 1% for hinges with t/R in the range of 0.02 to 0.1, and within 5% to 12% for thicker hinge with t/R in the range 0.2 to 0.6 (Tseytlin, 2002). However, both the full and simplified $\Delta\alpha_z$-compliance equations ($\Delta\alpha_z/M_z$) showed a large difference of up to 25% or more for t/R = 0.6 when compared to FEA and experimental results (Tseytlin, 2002). A comparison was conducted in this thesis between the experimentally determined rotational compliances ($\Delta\alpha_z/M_z$) of Smith *et al.* (1997) and the analytical compliances determined using the full and simplified equations of Paros and Weisbord. Experimental results of three flexure hinges with t/R = 0.125, 0.246 and 0.403 were available for comparison. Results of the comparison are shown in Table 2.1 below.

Flexure hinge (mm) b= 12.7mm	t/R	Exp. $\Delta\alpha_z/M_z$ (rad/Nm)	Analytical $\Delta\alpha_z/M_z$ (rad/Nm)			
			Full	% diff.	Simpl.	% diff.
t = 1.19, R = 9.53	0.125	0.0293	0.0304	3.8	0.0309	5.5
t = 2.34, R = 9.53	0.246	0.0059	0.0055	-6.0	0.0057	-3.0
t = 3.38, R = 9.53	0.403	0.0018	0.0016	-13.8	0.0017	-9.1

Table 2.1: Differences between the experimentally determined compliances ($\Delta\alpha_z/M_z$) of Smith *et al.* (1997) and the analytical compliances of Paros and Weisbord (1965)

It was expected that the full equation of Paros and Weisbord would be more accurate than that of the simplified equation. However, the results of the comparison revealed that the simplified equation provided better accuracies than that of the full equation for hinges with t/R = 0.246 and 0.403. It was also reported by Smith *et al.* (1997) that Paros and Weisbord's full equation of $\Delta\alpha_z/M_z$ provided larger differences than the simplified equation when compared to their FEA results for flexure hinges with $0.2 \leq t/R \leq 0.6$. From the results of these findings, it can be concluded that the accuracy of Paros and Weisbord's equations was ambiguous and unclear. Paros and Weisbord (1965) did not present FEA or experimental validations of their equations. Nonetheless, their equations have been widely applied in the design analysis of compliant mechanisms.

FEA approach was also used to estimate compliances of flexure hinges. Smith *et al.* (1987) derived an empirical equation of circular flexure hinges based on FEA results to predict only the rotational compliance, $\Delta\alpha_z/M_z$. However, they did

not experimentally verify the accuracy of their empirical equations or compared their results with that of Paros and Weisbord (1965). It was reported by Tseytlin (2002) that the empirical equation developed by Smith *et al*. was tractable and adequate only for thick hinges with t/R in the range of 0.2 to 1.0. Therefore, the accuracy of the empirical equation for thin hinges with small t/R ratios was unclear. Smith *et al.* (1987) did not derive empirical equations to predict the Δx- and Δy-compliances ($\Delta x/F_x$ and $\Delta y/F_y$) of flexure hinges.

Rong *et al.* (1994) derived analytical compliance equations of circular flexure hinges which can be reduced to the simplified equations of Paros and Weisbord (1965). They presented the compliance ratio of flexure hinges, which related the compliance in the axes of desired motion to compliances in the axes of undesired motion. Their equations were not verified with FEA or experimental results.

Her and Chang (1994) used the FEA approach to numerically determine the rotational stiffness ($M_z/\Delta\alpha_z$) of circular flexure hinges. A design graph of the normalised rotational stiffness for various t and R values was presented. Displacement analyses of two compliant micro-motion stages were presented. Displacements of the stages predicted using the FEA determined stiffness were significantly different from that predicted using the simplified equations of Paros and Weisbord (1965), especially for large t/R ratios. However, Her and Chang did not experimentally verify their results. They did not investigate the stiffnesses of flexure hinges in the x and y axes.

Xu and King (1995, 1996) used the FEA approach to analyse different flexure hinge profiles, which included the circular, elliptic and corner-filleted flexure hinges. They investigated the rotational deformations ($\Delta\alpha_z$) of hinges about the z-axis, the offset of the centre of hinges and the maximum stress of hinges during deformations. They found that circular flexure hinges provided only a small offset at the centre of the hinge during deformations when compared to the elliptical and the corner-filleted hinges. However, the circular flexure hinges were the least flexible which reduced the motion range of flexure hinges. They suggested that circular flexure hinges be used for applications that require a displacement of less than 0.1 mm with a small output force. They also found that elliptical flexure hinges have a lower accuracy than that of corner-filleted hinges; however elliptical hinges were able to achieve higher compliances with relatively lower maximum stress compared to both the corner-fillet and circular hinges. They verified the FEA model by testing a simple lever amplifier with flexure hinges. The difference between the FEA and the experimental output was less than 10%. Their papers focused on the analysis of different flexure hinge profiles; therefore analytical or empirical equations of predicting the hinge compliances were not presented.

Xu and Qu (1996) investigated the rotational stiffness of a limited number of circular flexure hinges with different t and R values using FEA software. They also analysed the effect of machining errors of flexure hinges on the displacements of a compound parallel stage. However, they did not compare their FEA results with previously derived analytical equations, such as equations derived by Paros and Weisbord (1965). Furthermore, they did not investigate stiffnesses of flexure hinges in the x and y axes.

Smith *et al.* (1997) studied both the compliance of circular and elliptical flexure hinges. They studied the differences between the full and the simplified $\Delta\alpha_z/M_z$ equations derived by Paros and Weisbord (1965). They found that Paros and Weisbord's full equation of $\Delta\alpha_z/M_z$ provided larger differences than the simplified equation when compared to the FEA results of Smith *et al.* (1997) for flexure hinges with $0.2 \leq t/R \leq 0.6$. This finding suggests that the accuracy of Paros and Weisbord's equations are ambiguous. Smith *et al.* derived closed-form analytical equations to predict the compliances of elliptical hinges based on a modification of Paros and Weisbord's equations. They compared their analytical results of elliptical flexure hinges with various dimensions to the FEA results. The maximum difference was 11.6%. They also experimentally verified their analytical equations and the maximum difference was 10%. They did not investigate the Δx- and Δy-compliances of flexure hinges.

Ryu and Gweon (1997) studied the motion errors of flexure hinge models induced by various types of machining imperfections such as drilling, reaming and wire-EDM processes. The compliance matrix of flexure hinges was obtained using equations derived by Paros and Weisbord (1965). Ryu and Gweon presented the effect of manufacturing errors on a simple compound stage. They demonstrated that the machining errors in the position and size of the holes of flexure hinges may cause significant in-plane motion errors, whereas machining errors in the perpendicularity of holes with respect to the plate may cause large out-of-plane motion errors.

Zhang and Fasse (2001) derived empirical equations based on FEA results to predict the $\Delta\alpha_z$-compliance of circular flexure hinges. Their empirical equations were expressed in terms of hinge dimensions and material properties. They compared their empirical results to Smith *et al.* (1987), Paros and Weisbord (1965) and to the unpublished results of Braak. The comparisons showed some differences between Zhang and Fasse's results and the others. Reasons for the differences were unclear. Zhang and Fasse did not experimentally verify the results of their empirical equations.

Wu and Zhou (2002) developed analytical compliance equations along all three

axes of circular flexure hinges. They compared their analytical results with the full and simplified equations derived by Paros and Weisbord (1965). Three flexure hinges with t/R ratios of 0.75, 1.143 and 0.257 were compared. Wu and Zhou's equations have the same results as Paros and Weisbord's full equations, except the signs of $\Delta\alpha_z/F_z$ and $\Delta y/M_z$ were opposite. This was due to the fact that Paros and Weisbord's equations were not concerned about the direction of forces, moments and deflections. Wu and Zhou also carried out comparisons between their compliance results with that of Paros and Weisbord's simplified equations, and Smith *et al.*'s equation (Smith *et al.*, 1987). Compliances calculated using Smith *et al.*'s equation and Paros and Weisbord's simplified equations showed significant differences from that of Wu and Zhou as t approaches R. Wu and Zhou did not verify their analytical results with that of FEA or experiments; therefore the accuracy of their equations was unclear.

Tseytlin (2002) derived the $\Delta\alpha_z$-compliance equations ($\Delta\alpha_z/M_z$) for both the circular and elliptical flexure hinges using the inverse conformal mapping method. Both circular and elliptical flexure hinges were classified into thin, intermediate and thick categories, and an equation was derived for each of the categories respectively. Tseytlin claimed that the conformal mapping equations were within 10% of the FEA and experimental results. However, the analytical equations were compared with experimental results only for circular flexure hinges with t/R in the range 0.02 to 0.1. Tseytlin compared the analytical results to that of Paros and Weisbord (1965) and Smith *et al.* (1987) for circular hinges with 0.2$\leq t/R \leq$0.5. Tseytlin's results were in close agreement to Smith *et al.*'s results, but were approximately 15% (when t/R= 0.5) different from that of Paros and Weisbord. Tseytlin compared Paros and Weisbord's full and simplified equation results ($\Delta\alpha_z/M_z$) with FEA and experimental results. The comparisons show that the full and simplified equations have large differences (up to 25% or more). Tseytlin also reported that the empirical equation derived by Smith *et al.* (1987) was adequate only for thick circular hinges with t/R in the range of 0.2 to 1. Tseytlin's work indicated that his new analytical equations provided better prediction of $\Delta\alpha_z/M_z$ than that of Paros and Weisbord and Smith *et al.* for 0.07$\leq t/R \leq$0.6. However, Tseytlin did not derive the Δx- and Δy-compliance equations of circular flexure hinges.

Lobontiu *et al.* (2001) derived analytical equations to predict the compliances of the corner-filleted flexure hinges along all three axes. Castigliano's second theorem was applied to derive the compliance equations. They compared compliances between the corner-filleted and the circular flexure hinges. It was found that corner-filleted hinges could deform more but induce lower stresses than that of circular hinges. However, the corner-filleted flexure hinges were less precise in

keeping their positions of the centres of rotation. Lobontiu *et al.* verified their analytical results of corner-filleted hinges with FEA and experimental results, and the differences were less than 10% and 6% respectively.

Lobontiu *et al.* (2002a) derived closed-form compliance equations for circular, elliptic, parabolic and hyperbolic flexure hinges. They considered only in-plane compliances in this paper. The compliance equations were derived using the Castigliano's second theorem. t/R ratios of circular hinges studied in this paper were 0.05, 0.1 and 0.2. Results of the analytical equations were compared with that of FEA (ANSYS). The results of the comparison reveal a 10% difference margin between FEA and analytical results. There were no experimental results presented in this paper. Lobontiu *et al.* (2002b) again presented the closed-form equations of parabolic and hyperbolic flexure hinges but this time they considered both the in-plane and the out-of-plane compliances. They also analysed the stress level of the parabolic and the hyperbolic hinges. FEA and experimental results were used to verify these analytical equations. Differences between analytical equations and FEA simulations were less than 8%. Differences between analytical and experimental results were within 4%. They also concluded that the parabolic flexure hinges were more compliant about the input axis and were subjected to less stress, whereas the hyperbolic flexure hinges were less sensitive to parasitic loading effects.

Lobontiu and Garcia (2003b) introduced a new class of flexure hinges, namely the axially-collocated and symmetric two-axis flexure hinges. This new class of flexure hinges have two sensitive axes which define the main rotational motions of the hinges. Generic mathematical equations were derived to predict the compliances of these hinges. Numerical analyses were carried out on parabolic-profile two-axis flexure hinges. Analytical results were compared to FEA simulation results and differences were less than 6%. There were no experimental data presented to verify the analytical equations.

Schotborgh *et al.* (2005) presented dimensionless graphs for three types of flexure hinge, namely circular, beam and cross hinges. Results of these dimensionless graphs were obtained using FEA simulations (ANSYS). The t/R range of the dimensionless graphs was from 0 to 2. These dimensionless graphs were used to obtain stiffnesses and stresses of flexure hinges in various axes. However, they did not compare the results of the dimensionless graphs with the previously derived analytical equations. They also did not conduct experiments to verify the accuracy of these dimensionless graphs.

2.1.1 Gaps in current knowledge of the modelling of flexure hinges

A few conclusions can be drawn from all the above work regarding the modelling of flexure hinges with various profiles. Circular flexure hinges provide accurate rotational motions in terms of keeping their positions of the centre of rotation as reported by Xu and King (1995, 1996) and Lobontiu *et al.* (2002a). Circular flexure hinges are suitable for applications requiring precision and predictable motions. Therefore, micro-motion stages studied in this thesis utilise only circular flexure hinges.

There were various compliance equations available for circular flexure hinges. A few research studies (Smith *et al.*, 1987; Her and Chang, 1994; Smith *et al.*, 1997; Zhang and Fasse, 2001; Tseytlin, 2002; Lobontiu *et al.*, 2002a; Schotborgh *et al.*, 2005) conducted comparisons of their analytical or empirical compliance equations with their FEA results. However, there were only two research groups (Smith *et al.*, 1997; Tseytlin, 2002) who experimentally verified their analytical or empirical equations of circular flexure hinges. Furthermore, there were not many researchers who compared their analytical or empirical results with the previously derived equations. Zhang and Fasse (2001) compared their empirical results with that of Smith *et al.* (1987). However, it was reported by Tseytlin (2002) that Smith *et al.*'s equation was accurate only for flexure hinges with t/R in the range of 0.2 to 1. Therefore, the comparison conducted by Zhang and Fasse (2001) was valid only for $t/R \geq$0.2. Tseytlin (2002) compared analytical results with that of Paros and Weisbord (1965) and Smith *et al.* (1987) for circular hinges with t/R in the range of 0.2 to 0.5. Tseytlin's results were close to that of Smith *et al.*; however the comparisons above were carried out for the $\Delta\alpha_z$-compliance of flexure hinges only. There was no literature review up to this date reporting the comparison of all three in-plane compliance equations, $\Delta x/F_x$, $\Delta y/F_y$ and $\Delta\alpha_z/M_z$ for a wide t/R range of circular flexure hinges.

Some of the previously derived analytical/empirical compliance equations provide better accuracies than others depending on the t/R ratios of circular flexure hinges. Flexure hinge compliances derived by any particular research group may not be accurate for a large range of t/R ratios. These two issues can be observed from the result of comparisons conducted by Tseytlin (2002). There is a lack of literature reporting the accuracy of the previously derived hinge equations for a wide range of t/R values. There was also no proper scheme developed to guide designers on how to select the most suitable flexure hinge equation out of the previously derived analytical or empirical equations. Therefore, this thesis investigates the

accuracy of various hinge compliance equations for a large range of t/R ratios ($0.05 \leq t/R \leq 0.8$), and proposes a scheme for selecting the most suitable hinge equation based on the t/R ratio.

2.2 Modelling of compliant micro-motion stages

As mentioned in the introductory chapter, it is more complicated to model the kinematics and statics of compliant stages precisely compared to the well understood rigid-body mechanisms with simple revolute joints. This was partly due to the fact that flexure hinges possess more than one-DOF. Unlike revolute joints which have only the rotational motions about the z-axis, flexure hinges have both translational and rotational motions in the x, y and z axes, resulting in a total of six-DOF.

Circular flexure hinges are designed to predominantly provide one-DOF, namely the rotational motions, $\Delta\alpha_z$ about the z-axis only. Therefore the simplest technique used to model a compliant mechanism is to model flexure hinges as having only one-DOF. The PRBM method is widely used to predict the displacements of compliant mechanisms with flexure hinges. The PRBM commonly models a flexure hinge as a revolute joint (one-DOF) with an attached torsional spring. However, flexure hinges do not provide purely rotational motions. Flexure hinges have other DOFs as shown in Figure 2.1. Although the PRBM method is effective and it simplifies the model of compliant mechanisms, the PRBM suffers some inaccuracies when it ignores the other DOFs of flexure hinges.

For planar compliant micro-motion stages, circular flexure hinges are commonly modelled to have only the in-plane DOFs, which are the translation motions (Δx and Δy) in the x and y axes, and the rotational motions ($\Delta\alpha_z$) about the z-axis. This simplification is made because circular flexure hinges possess high out-of-plane stiffnesses (Smith *et al.*, 1997). Out-of-plane motions of circular flexure hinges are small and therefore can be neglected.

Scire and Teague (1978) developed a one-DOF compliant stage for the use of optical and electron microscopes in the microelectronics industry. Initially, they derived an equation using the PRBM method to predict the kinematics and the amplified output displacements of the stage. However, the predicted total displacement gain of the stage was 30.3 while the measured gain was only 16.9. The equation derived using the PRBM was not accurate as the stage was over-constrained and it led to the Δx- and Δy-deformation of flexure hinges. Scire and Teague improved their model where they considered axial strain (in the x-axis) in the most stressed hinge. They used the simplified hinge equations developed by Paros and

NOTE: This figure is included on page 18 of the print copy of the thesis held in the University of Adelaide Library.

Figure 2.1: Flexure hinge (Handley, 2006)

Weisbord (1965) to model the flexure hinge compliances. The model showed a significant improvement. However, they only considered the Δx-deformation on the most stressed hinge while ignoring the Δx-deformation of the remaining flexure hinges. Furthermore, they did not include the Δy-deformation of hinges in their model. The static model of compliant stages was not presented.

Han et al. (1989, 1991) presented the modelling and optimal design of a six-DOF parallel micromanipulator using a Stewart Platform. A kinematic model was derived based on the PRBM method, the kinematic influence coefficient concept and the virtual work principle. Flexure hinge compliances were derived and analysed using the Castigliano's theorem; however only the rotational DOF of flexure hinges was considered. The kinematic model was not experimentally verified.

Furukawa and Mizuno (1990) predicted the kinematics and statics of a one-DOF compliant mechanism. The mechanism was used as both a magnifying and reducing mechanism. The kinematic and static models were first derived using the PRBM method and later incorporated the Δx-compliance of flexure hinges to improve the modelling accuracy of the compliant mechanism. The input and output displacements were measured during experiments and their results were in good agreement with the analytical values. However, the static model was not experimentally verified and the accuracy of this model is unclear.

Rong et al. (1994) investigated the design of a one-DOF compliant micro-motion stage. They investigated the manufacturing error effects of the stage by carrying

out some simple analysis using the PRBM method. However, they did not derive kinematic and static models of the one-DOF micro-motion stage. Therefore, no comparisons were made among the analytical, FEA and experimental results.

Her and Chang (1994) developed a linear scheme for displacement analysis of compliant stages with flexure hinges. The scheme was developed based on the PRBM method and the linearisation of the geometric constraint equations of a compliant structure. The principle of virtual work was incorporated into the scheme to provide additional constraint equations to solve all unknowns. Rotational stiffnesses of flexure hinges were found using a commercially available FEA software. They claimed that the obtained stiffnesses from the FEA model were more accurate than the commonly used simplified equations derived by Paros and Weisbord (1965). Their method did not consider the Δx- and Δy-deformations of flexure hinges. The maximum displacement differences of the linear scheme method was about 20% when compared to their FEA results. The accuracy of this linear scheme method was not experimentally verified. Her and Chang also applied their analytical modelling method on an over-constrained mechanism (similar to the mechanism presented by Scire and Teague (1978)). They stated that a link must deform for such an over-constrained structure. However, it was more likely that the hinges deformed in the Δx- and Δy-directions before the linkages deformed (Handley, 2006). Such hinge deformations were not modelled by the linear scheme method. This could explain the differences between the linear scheme and FEA results. The static model of the compliant stage was not presented.

Furukawa *et al.* (1995) analysed the kinematics, statics and dynamics of a one-DOF translational stage with circular flexure hinges. The PRBM method was initially used to predict the amplification of the mechanism. They found that the amplification ratio of the stage was reduced due to the Δx-deformation of flexure hinges. Therefore, they incorporated the effects of the Δx-deformation of hinges in the PRBM. They used the compliance equations of circular flexure hinges derived by Paros and Weisbord (1965) to calculate the $\Delta\alpha_z$- and Δx-compliances of flexure hinges. The Δy-compliances of flexure hinges were not considered in their formulations. They experimentally verified their results and claimed that the predicted amplification of the mechanism was in close agreement to the experimental results; however the differences were not presented.

Yang *et al.* (1996) developed a piezo-driven vertical motion compliant stage for the use in laser-welding. An analytical model for statics estimation of the stage was derived based on the PRBM method. The statics of the compliant stage was obtained through force balancing. The Δx-deformation of hinges was not considered initially. The $\Delta\alpha_z$-compliances of flexure hinges were calculated based on the

simplified equation of Paros and Weisbord (1965). The analytical model showed a significant difference, up to 30% when compared to their FEA results. Further investigation revealed that the heavily stressed hinge experienced deformations in the x-axis of flexure hinges. Therefore, a modified model was derived which considered the Δx-deformation of the heavily stressed hinges. The modified analytical results were compared to their FEA model and the difference was only 2%. The stiffness of the stage was experimentally verified. The experimentally determined stiffness was 5% lower than the FEA predicted value. Their analytical model did not include the Δy-deformation of flexure hinges; therefore this deformation effect on the static behaviour of the stage was unclear.

Shim *et al.* (1997) derived a kinematic model of a six-DOF parallel micromanipulator for micro-positioning applications. The model was derived using the PRBM method; therefore flexure hinges were modelled to have only one-DOF. They investigated the workspace and singularity of the micromanipulator using the derived kinematic model. However, they did not compare the analytical model with FEA simulations or experimental results. Therefore, the accuracy of the model was unclear.

Lee and Kim (1997) presented a XYθ precision stage for the alignment of wafers in microlithography. A kinematic model was derived to relate the elongations of piezo-actuators to the output displacements of the stage. This model was used with a proportional-integral-derivative (PID) controller for the control of positioning. The positioning resolution for the x and y motions was approximately 10 nm, while the resolution of the θ motion was 0.114 arcsec. However, the accuracy of the kinematic model was not experimentally verified. Lee and Kim's paper focused on the design and control of the precision stage. There was no static model presented to estimate the stiffness of the stage.

Chang and Du (1998) designed a one-DOF micropositioner compliant stage using multiple Scott-Russell linkages. They derived equations to relate the input and output displacements of the mechanism using the PRBM method. The Δx- and Δy-compliances of flexure hinges were not considered in the equation. The derived input-output displacement equation was used in the optimisation technique (named the Taguchi method) as a control factor to find an optimised configuration of the micropositioning stage. A two-dimensional FEA model was used to analyse displacements for 27 different control factor settings. Experiments were carried out to measure the amplified output displacements of the mechanism. According to the optimised results, the amplification gain of the mechanism was expected to be 20; however the observed gain was only 9.66 during their experiments. They claimed that the differences were attributed to a) the reaction force produced by the

leaf springs which reduced the overall displacements of the piezo-actuator, and b) the bending of linkages which reduces the output displacement of the stage. However, the differences could also be attributed to the unmodelled DOF, which were the Δx- and Δy-deformations of flexure hinges, but it was not discussed by Chang and Du. Therefore, the effect of these unmodelled DOF on the amplification of the micropositioning stage is unclear.

Gao *et al.* (1999) derived a static model for a two-DOF compliant stage. The Δx-deformation of flexure hinges was considered in these models. Paros and Weisbord's simplified equations were used to calculate the $\Delta \alpha_z$- and Δx-compliances of flexure hinges. Therefore, the accuracy of the static model was dependent on the accuracy of the simplified hinge equations. The static model was derived through the equilibrium of forces. The maximum difference of stiffness between analytical and experimental results was approximately 14%. Gao and Swei (1999) also developed a six-DOF micro-motion stage. This stage used a 3-RRR (revolute-revolute-revolute) and a 3-PRP (revolute-prismatic-revolute) stage to provide the six-DOF motions. A forward and inverse kinematics of the stage were derived using the PRBM and the assumption of small angle approximations. The derived kinematic model was expressed in the form of a constant Jacobian matrix. However, the kinematic model did not consider the Δx- and Δy-deformations of flexure hinges. Static analysis of the stage was not presented. The results of the kinematic model were not compared with the FEA and experimental results; therefore the accuracy of the model is unclear.

Chang *et al.* (1999a) developed a three-DOF micropositioner for ultraviolet lithography applications. The micropositioner consists of a XY stage and a θ_z stage attached on top of the XY stage. Four piezo-actuators were installed at the XY stage to provide the two translational motions and two piezo-actuators were installed at the θ_z stage to provide the rotational motions. Details of the analytical modelling procedures were not presented. A FEA (ANSYS) model was developed to simulate the static and dynamic behaviour of the micropositioner for comparison purposes. The static performance of the micropositioner was experimentally verified (Chang *et al.*, 1999b). Static displacements of the micropositioner were obtained when piezo-actuators were driven at 100V. When compared to the FEA, the maximum difference of static displacements was 2.7% along the y-axis. When compared to the experimental results, the maximum difference of static displacements was 7.9% about the θ_z-axis. The analytical model of the micropositioner showed good accuracy when compared to FEA and experimental results. However, these accuracies were achieved using six piezo-actuators compared to most of the three-DOF structures which used only three piezo-actuators. The kinematic

model of the micropositioner was not presented.

Ryu *et al.* (1997) developed a $XY\theta$ compliant stage which was driven by three piezo-actuators. The topology of this stage is similar to a 3-RRR mechanism except it consists of a double compound lever at each of the three input linkages. These double compound levers act as an amplification lever to provide mechanical displacement gain. They formulated a kinetostatic model to describe the relationship between input and output displacements, and stiffnesses of the stage by considering compliances of flexure hinges in all three axes. The analytical results were compared with experimental results. By comparing the predicted and measured output motions, the difference in the x-axis was 29%, the difference in the y-axis was 36% and the difference of rotational motions about the z-axis was 11%. They claimed that these differences may be caused by the machining errors of the stage as well as analytical modelling errors. Ryu *et al.* (1999) also showed that a calibration was required to improve the kinematic model; therefore it could be use for open-loop position control with a 5% positioning error. The methodology presented by Ryu *et al.* (1997) of deriving the kinetostatic model was complicated and involved an intensive number of coordinate transformations. They experimentally verified the kinematics of the model; however they did not verify the static results with that of FEA or experiments. Therefore, the accuracy of the static estimations of this kinetostatic model is unclear.

Ohya *et al.* (1999) developed a spatial three-DOF micro-manipulator using circular and spherical flexure hinges. The inverse kinematics of the device was derived using conventional robotics and the PRBM method. Their model did not consider the Δx- and Δy-deformations of flexure hinges. They did not compare the analytical model with FEA or experimental results. The analytical model was not used for control purposes. They presented a calibration process to obtain the Jacobian matrix and this experimentally determined Jacobian was used for control instead. The accuracy of the derived kinematic model is unclear. They did not present the static model of the device.

Gao *et al.* (2000) designed an ultra-precision stepping positioner with a displacement resolution of over 10 nm. They derived an analytical static model to predict the stiffness of the positioner. However, they only considered the $\Delta\alpha_z$-compliance of flexure hinges in their models. The effect of the unmodelled Δx- and Δy-compliances on the performance of the stage is unclear. Experiments were carried out to measure the resolution and the natural frequency of the positioner. The experimentally determined natural frequency was in close agreement with the analytical result.

Hsiao and Lin (2001) derived a static model for a RRR compliant stage with

three flexure hinges. They derived a relationship between external applied loads and deflections at the loading point. One-dimensional beam theory and the Castigliano's theorem were used to determine the deformations of the stage. A FEA model was developed for comparison purposes. The maximum difference between the FEA determined compliance and analytical compliance was 8.5%. The analytical model was also experimentally verified. Differences were within 14% in the case of horizontal loading while differences were within 18% in the case of vertical loading. They also presented the effect of various flexure hinge dimensions to the compliance of the RRR structure. However, their modelling method was not used to model other closed-loop compliant mechanisms, such as a simple compound stage with a four-bar linkage topology and a 3-RRR compliant mechanism. It is not clear if this method would be applicable to those type of mechanisms.

Chung *et al.* (2001) developed a spatial three-DOF micro-motion stage for teleoperations to manipulate microscopic objects. They derived the forward and inverse kinematic models of the stage based on the PRBM model. The forward kinematic model was compared with the FEA simulations and the kinematic results were in close agreement with the FEA results. However, the kinematic results were obtained by using the flexure hinge deformations obtained from the FEA simulations of the stage. Therefore, the analytical kinematic models were relied on the FEA simulations of this particular stage. The kinematic model was not experimentally verified. A static model of the stage was not presented.

Elmustafa and Lagally (2001) designed a one-DOF nanopositioner for the use in precision machining such as the CNC milling machine. The nanopositioner consists of four beam-type flexure hinges. The stage was designed to have a high stiffness and a large load carrying ability. A static analysis was carried out using FEA simulations. Graphs of selection of design parameters to meet certain requirements were produced through the static analysis. There was no analytical models presented to predict the kinematic and static performances of the stage.

Zhang *et al.* (2002) developed a 3-RRR compliant stage. The topology of this stage was the same as the topology studied in this thesis. A kinematic model of the stage was derived based on the PRBM and the Δx- and Δy-deformations of flexure hinges were not considered in the model. They linearised the kinematic model using a Taylor series expansion for the derivation of the displacement variables. This method was feasible as the displacement of links were sufficiently small. Experiments were conducted to verify the accuracy of the kinematic model. However, a comparison revealed significant differences between the model and experimental results. Therefore, calibrations were carried out to improve the accuracy of the kinematic model. The calibrated kinematic model would not be applicable for

other 3-RRR mechanisms with different geometries and flexure hinge dimensions. A static model of the 3-RRR compliant mechanism was not presented in this paper.

Koseki *et al.* (2002) derived a kinematic model for a translational three-DOF micro-parallel mechanism using a matrix method. The matrix method assumed that a) the relationship between forces and deformations are linear (Hook's Law) and b) the translational and rotational displacements are small enough to be linearised. They claimed that the matrix method was well suited to model circular flexure hinges in their mechanism. The method modelled both the compliances of flexure hinges and beam elements in all three axes. Therefore the kinematic model was expected to provide good accuracies. However, this was not the case. The kinematic model, in the form of a constant Jacobian matrix which described the relationship between the input and output displacements, was compared to an experimentally determined Jacobian matrix. The comparison revealed significant differences where the differences between the Jacobian terms were more than 50%. They suggested that some errors might be attributed to the friction between the three piezo-actuators and the mechanism. A static model of the compliant mechanism was not presented.

Pham and Chen (2002) presented a two-DOF parallel compliant mechanism with flexure hinges. They derived the kinematic and static models of the mechanism based on the PRBM method and flexure hinges were modelled to have only one-DOF. They compared the results of the models with FEA simulations. The differences between the analytical model and the FEA simulations were 1% for the displacements and 3% for the holding forces of the actuators. However, they did not derive equations to estimate the stiffnesses of the end-effector. They did not experimentally verify their models.

Jouaneh and Yang (2003) developed a kinetostatic model to predict the displacement and stiffness of the same vertical motion compliant stage as Yang *et al.* (1996). The displacement ratio between the input and output motions of one of the levers, together with the stiffness at either end of this lever were firstly obtained. The overall displacement and stiffness of the compliant stage were then obtained by combining the individual results from each lever. The developed equations modelled flexure hinges as having multi-DOF, namely the Δx-, Δy- and $\Delta\alpha_z$-deformations. The analytical results were compared with both the FEA and experimental results. The differences between the analytical and the FEA results were 3.1% for displacement and 1.3% for stiffness of the compliant stage. The differences between the analytical and the experimental results were 10.4% and 6.7% respectively for displacement and stiffness of the compliant stage respectively. By incorporating the effects of the Δx- and Δy-deformations of hinges in the kine-

tostatic model, differences of the stiffness prediction of the compliant stage were reduced from 10% to 6.7% when compared to experimental results. This showed the significance of modelling flexure hinges as having multi-DOF. The kinetostatic modelling method was applied on a one-DOF compliant stage. It was not clear if this method would be applicable to multi-DOF compliant stages such as 3-RRR compliant micro-motion stages.

Lobontiu and Garcia (2003a) formulated an analytical method for displacement and stiffness calculations of planar compliant mechanisms with flexure hinges. The closed-form formulations were based on strain energy and Castigliano's displacement theorem which considered all three in-plane compliances of hinges. The closed-form equations were expressed as a load-deformation relationship. The displacement, input stiffness and output stiffness equations of a one-DOF compliant mechanism were expressed as a function of geometry and material properties. Differences between analytical and FEA (ANSYS) results were 5%, 3.2% and 4.9% for displacement, input stiffness and output stiffness respectively. However, there was no experimental results to further justify the accuracy of the analytical method. The modelling method was not applied to multi-DOF compliant mechanisms such as 3-RRR micro-motion stages and it is not clear if this method would be applicable to these type of mechanisms.

Yi *et al.* (2003) developed a kinematic and a stiffness model for a 3-RRR compliant stage. They modelled the first flexure hinge of each RRR chain to have two-DOF, which were the $\Delta\alpha_z$- and Δx-displacement. This solution resulted in a compliant stage mobility of six, and six piezo-actuators were required to control the stage. They derived the kinematic and stiffness models for a three-mobility (conventional 3-RRR structure driven by three piezo-actuators) and a six-mobility compliant stage. The analytical displacements were compared with FEA results. The six-mobility model results were significantly closer to the FEA results compared to that of the three-mobility model. Experiments were also conducted to measure the stiffness of the compliant stage. The differences were 2.6% for the stiffness in the x and y axes. However, the difference was 31% for the rotational stiffness about the z-axis. These accuracies were achieved with six piezo-actuators instead of the conventional three piezo-actuators. Extra piezo-actuators increase expenses and control complications to a system. Furthermore, only three out of nine flexure hinges were modelled to have two-DOF. The unmodelled DOFs at the other six flexure hinges may introduce errors to the model. The Δy-deformation of flexure hinges was not considered in their models.

Liu and Li (2002) derived a kinematic and a dynamic model for a three-DOF parallel compliant stage. This compliant stage consists of four-bar linkages as the

driving structures. Their models only considered the $\Delta\alpha_z$-deformations of flexure hinges. The Δx- and Δy-deformations were ignored. The accuracies of the analytical models were unclear because the models were not compared to FEA or experimental results.

Yu *et al.* (2004) derived a kinematic model for a three-DOF compliant micromotion stage. The design of this mechanism was based on a modified DELTA mechanism. The kinematic model was derived based on the PRBM concept and flexure hinges were modelled to have only one-DOF. An analytical constant Jacobian matrix was obtained. However, the analytical Jacobian showed significant differences when compared to an experimental Jacobian. The reason for the large difference was not explained. Calibrations were carried out to obtain an experimental Jacobian matrix for positioning control purposes. Yu *et al.* (2004) did not derive a more accurate kinematic model nor quantify the error in their kinematic model. Therefore, their approach of deriving the kinematic model is still questionable.

Wu and Zhou (2004) developed a $XY\theta$ compliant mechanism which was driven by only one actuator, resulting in a smaller and more compact mechanism compared to other three-DOF mechanisms with three or more actuators. The principle of inchworm movement was adopted to actuate the mechanism. Experiments were carried out to measure the displacement of the mechanism. Although only one actuator was required in this mechanism to provide three-DOF motions, the motions were coupled to each other. Therefore, this mechanism could not provide pure translational or rotational motions. There was no analytical model presented in this paper.

Culpepper and Anderson (2004) designed the *HexFlex*^{TM}, a six-DOF nanomanipulator which utilises beam-type flexures. The nanomanipulator was driven by two-axis electromagnetic actuators. The symmetrical characteristic of the design made the nanomanipulator insensitive to thermal expansion. The geometry of the compliant mechanism was designed using the *CoMeT*^{TM} (Compliant Mechanisms Tool), which is a design tool developed at the MIT Precision Compliant Systems Laboratory. The *CoMeT*^{TM} design tool was written in Matlab and the beam theory was used to calculate the kinematics and statics of compliant mechanisms. The displacements of the *HexFlex*^{TM} compliant mechanism calculated using the *CoMeT*^{TM} was experimentally verified and the differences were within 14%. However, beam-type flexures were used in the six-DOF nanomanipulator design. The accuracy of using the *CoMeT*^{TM} to calculate the deformation of nanomanipulators with circular flexure hinges is unclear.

Park and Yang (2005) developed a monolithic six-DOF ultra precision position-

ing compliant mechanism driven by six piezo-actuators. They derived a kinetostatic model using the Castigliano's second theorem to describe the relationship between displacements and forces applied at the end point of flexure hinges. The flexure hinges were modelled to have six-DOF. Relative displacements between flexure hinges were calculated using vector analysis. A stiffness matrix of the compliant mechanism was derived using the least action principle. The relationship between the input and the output displacements was also derived. Results of this relationship were compared with FEA results; for translational motions, the differences were 28% along the x-axis and 29% along the y-axis, and for rotational motions, the differences were 17% about the x-axis, 23% about the y-axis and 13% about the z-axis. Stiffnesses of the compliant mechanism were not verified with FEA models. The accuracy of the kinetostatic model was not experimentally verified.

Kim *et al.* (2005) designed a flexure hinge-based XYZ scanning stage for an atomic force microscopy scanner. They carried out an optimisation analysis based on the approach of Ryu *et al.* (1997). Their main objective was to design a scanning stage with minimum Abbe errors. Flexure hinges were modelled to have six-DOF. The compliance equations derived by Paros and Weisbord (1965) were used to calculate the compliances of flexure hinges. A FEA model was generated to compare with the analytical model. The full range displacement differences were 8.9% and 4.9% in the x- and y-axis respectively. The comparison of the full range displacements in the z-axis was not presented. The predicted full range displacements were not compared to experimental results. They conducted experiments to investigate the Abbe errors of the stage. Results showed that the stage had small Abbe errors. They did not derive formulations to describe the relationship between the input and output displacements nor to estimate the stiffnesses of the scanning stage.

Choi and Lee (2005) developed a six-DOF compliant wafer stage for nano-imprint lithography, which requires surface contact between a template with nano patterns and a wafer that transfers the patterns. Beam-types and L-shape flexures were used in the wafer stage design to provide the required deformations. A dynamic model was derived to aid the stiffness analysis of the wafer stage. Experiments were conducted on the wafer stage in a nano-imprint machine, and nano patterns with line widths of 100 and 86 nm were transfered successfully. However, they did not present experimental results to verify the analytical stiffness results of the structure.

Ma *et al.* (2006) presented an analysis of the amplification ratio of a one-DOF compliant mechanism which has the same topology as studied by Lobontiu and

Garcia (2003a). Bridge-type flexure hinges were used in the mechanism to provide the required deformations. The bridge-type flexure hinges were modelled to have six-DOF. The estimated amplification ratios of the mechanism were significantly different from the FEA results (by a factor of two approximately) for certain link arrangements of the mechanism. They did not derive equations to estimate the input and output stiffnesses of the mechanism. The method was not applied to multi-DOF compliant mechanisms such as 3-RRR micro-motion stages and it is not clear if this method would be applicable to these type of mechanisms.

Choi *et al.* (2006) derived a formulation using the Lagrange's equation to predict the amplification ratio of a one-DOF compliant mechanism with circular flexure hinges. They modelled flexure hinges to have six-DOF which included the out-of-plane DOF. The predicted amplification ratio was 22. Experiments were conducted to measure the amplification ratio of the mechanism. The measured ratio varied from 18.6 to 21.9. The differences between the analytical and the experimental results were approximately 10%. They suggested that the differences between the analytical and the experimental results were due to the fabrication errors, the experimental errors and also due to the fact that the Poisson's ratio of the steel did not feature in their proposed analytical model. The input and output stiffnesses of the mechanism were not presented. The modelling method was not applied to multi-DOF compliant mechanisms such as 3-RRR micro-motion stages and it is not clear if this method would be applicable to those type of mechanisms.

Pham *et al.* (2005) derived a kinematic model of a three-DOF flexure parallel mechanism (FPM) using an extended PRBM method, named the PRB-D method. The FPM consists of three double compound linear structures (one-DOF mechanism) and three 3-RRR compliant mechanisms (three-DOF mechanism) in order to achieve three-DOF. The PRB-D method models flexure hinges to have six-DOFs. They used the PRBM and PRB-D kinematic results to control the mechanism and the PRB-D results produced 1/3 the error of the PRBM results. The input and output compliances of the mechanism were not presented.

Pham and Chen (2005, 2006) derived analytical models to estimate the output stiffnesses of the same FPM aforementioned. The method of deriving the stiffness model involved an intensive number of transformation matrices. This method could lead to complications and difficulties when it is applied to other mechanisms. The analytical output stiffnesses of the FPM were compared to the FEA and experimental results and the differences were within 10%. The input stiffness of the FPM was not presented and it was not clear if this methodology can be used to estimate the input stiffness of compliant mechanisms.

Choi and Kim (2006) designed a two-DOF linear compliant mechanism with beam-type flexures. They derived a mathematical model to analyse the deformation and natural frequencies of the mechanism. A FEA model was generated using ANSYS for comparison with the analytical values. They claimed that the analytical and the FEA results were in close agreement. However, their modelling method was used to model a compliant mechanism with beam-type flexures. The accuracy of using their model to calculate the deformation of compliant mechanisms with circular flexure hinges is unclear.

Handley (2006); Handley *et al.* (2006) developed a Simple-Compliant-Hinge-Model (SCHM) using ANSYS to model flexure hinges of compliant mechanisms to have three-DOF. Flexure hinges were modelled using two coincident nodes joined by two elements, which were the COMBIN7 and COMBIN14 elements. The COMBIN7 provides a three-dimensional revolute joint with stiffnesses, whereas the COMBIN14 provides extra stiffness in the x-direction to the hinge model. These SCHM of flexure hinges were connected using BEAM3 elements to generate various topologies of compliant mechanisms. The SCHM method was used to estimate the kinematics, input and output stiffnesses of 3-RRR micro-motion stages. The SCHM method is a numerical kinetostatic model and it was shown to be computational efficient. The SCHM results were verified with two-dimensional FEA models and experimental results. The Jacobian (kinematics) results of the SCHM were within 2% in translational motions and 27% in rotational motions when compared to the FEA and the experimental results respectively. However, the SCHM method requires a FEA simulation which may be expensive. Therefore, analytical kinetostatic models are preferred as an alternative to the FEA dependent models.

2.2.1 Gaps in current knowledge of the kinetostatic modelling of compliant micro-motion stages

There were various kinetostatic models previously derived to predict the kinematic and static performances of micro-motion stages. However, most of the models were derived based on the PRBM method where flexure hinges were modelled to have only one-DOF. A few research groups modelled some or all flexure hinges to have two-DOF, which were the $\Delta\alpha_z$- and Δx-deformations. However, the Δy-deformation of flexure hinges was ignored. This unmodelled DOF could introduce inaccuracies in the analytical model.

There were only a few research groups who derived kinetostatic models which modelled circular flexure hinges to have three-DOF or more (Jouaneh and Yang, 2003; Ryu *et al.*, 1997; Lobontiu and Garcia, 2003a; Park and Yang, 2005; Choi *et al.*,

2006; Pham and Chen, 2005; Handley, 2006). However, except for Jouaneh and Yang (2003), Ryu *et al.* (1997), Choi *et al.* (2006), Pham and Chen (2005) and Handley (2006), these research groups did not experimentally verify the kinetostatic models. Jouaneh and Yang (2003), and Choi *et al*. (2006) applied their modelling methods on a one-DOF of micro-motion stage, however they did not apply their modelling method on multi-DOF compliant structures such as 3-RRR micro-motion stages. It is not clear if these methods would be applicable to those type of mechanisms. Ryu *et al*. (1997) modelled a compliant stage similar to a 3-RRR mechanism except it consists of a double compound lever at each of the three input linkages. Their method involved an intensive number of coordinate transformations, and therefore may be complicated. They experimentally verified the kinematic model; however they did not verify the stiffnesses of the stage. Therefore, the accuracy of the stiffness predictions of the kinetostatic model is unclear. Pham and Chen (2005) modelled the kinetostatics of a three-DOF flexure parallel mechanism (FPM) which consists of three 3-RRR compliant mechanisms and three double compound linear structures. Their method involved an intensive number of transformation matrices. This method could lead to complications and difficulties when it is applied to other mechanisms. The input stiffness of the FPM was not presented and it is not clear if this methodology can be used to estimate the input stiffness of compliant mechanisms. The prediction of the input stiffness was particularly important for the design of piezo-driven compliant mechanisms because the maximum displacement of a piezo-actuator is governed by the structural input stiffness. High input stiffnesses reduce the maximum displacement of a piezo-actuator, which leads to the reduction of the workspace of compliant mechanisms (Handley, 2006). The SCHM method of Handley (2006) relied on a FEA simulation software such as ANSYS. Although the SCHM method was more computational efficient than a two- or three-dimensional FEA model, an analytical kinetostatic model would be preferred as an alternative modelling method because FEA simulation software is relatively expensive.

As a conclusion, a simple analytical kinetostatic modelling method which can be used to predict the kinematics, and both the input and output stiffnesses/ compliances of compliant mechanisms, especially for 3-RRR micro-motion stages has still not been studied in great detail.

2.3 Summary

There are two main gaps identified in the area of the modelling of compliant micro-motion stages that lead to the main objectives of this thesis:

- there is no proper scheme developed for selecting the most suitable flexure hinge equation based on the t/R ratio of flexure hinges; and
- the kinetostatic modelling of compliant mechanisms, especially the 3-RRR micro-motion stages, has still not been studied in great detail.

CHAPTER 3

A Scheme for Selecting Flexure Hinge Compliance Equations

Prior to the development of a scheme for selecting the most suitable circular flexure hinge compliance equation, it is necessary to investigate the accuracy and limitation of previously derived hinge equations (Paros and Weisbord, 1965; Lobontiu, 2003; Wu and Zhou, 2002; Tseytlin, 2002; Smith *et al.*, 1987; Schotborgh *et al.*, 2005; Zhang and Fasse, 2001). The investigation requires that the result of hinge equations be compared to either FEA or experimental results. However, it is impractical to conduct experiments for a large number of flexure hinges with different t/R ratios. Therefore, FEA results generated using ANSYS were chosen to serve as a benchmark for comparisons in this thesis. In order to ensure that the FEA determined compliances well represent the actual compliances of flexure hinges for a wide range of t/R ratio, experiments were carried out to measure the compliances of three flexure hinges from each of the categories of thin ($t/R \leq 0.07$), intermediate ($0.07 < t/R \leq 0.2$) and thick ($0.2 < t/R \leq 0.8$). These categories were defined to be the same as that of Tseytlin (2002). The FEA results were compared to the experimental results and the differences are presented in this chapter. The FEA results were in close agreement to the experimental results; therefore the FEA model was appropriate to serve as a benchmark for comparisons.

For further justification of the accuracy of the FEA results in this thesis, the FEA results were also compared to the experimental results of Smith *et al.* (1997). Smith *et al.* (1997) conducted experiments to measure the $\Delta\alpha_z$- compliances of three flexure hinges from the intermediate and thick hinge categories. The FEA results in

this thesis were in close agreement to the experimental results of Smith *et al.*; therefore the FEA model was adequate and appropriate to serve as a benchmark for comparisons.

Flexure hinge compliance equations which were studied in this chapter include equations derived by Paros and Weisbord (1965) (both full and simplified), Lobontiu (2003), Wu and Zhou (2002), Tseytlin (2002), Smith *et al.* (1987), Schotborgh *et al.* (2005) and Zhang and Fasse (2001). The results of these analytical and empirical equations were compared to FEA results. Graphs of differences between the analytical/empirical and FEA results versus t/R ratios of flexure hinges were presented. The differences were analysed, and thus a scheme for selecting the most suitable flexure hinge equations based on the t/R ratio was developed.

3.1 Modelling of circular flexure hinges using FEA

ANSYS was used to construct FEA models of flexure hinges. These flexure hinge models were generated using 8-node, two-dimensional, plane elements (PLANE82) with two-degrees-of-freedom on each node (which are the translations in the nodal x and y directions). This element type is well-suited to model irregular shapes and curved boundaries without much loss of accuracy (ANSYS, 2002). The thickness of the model was taken into consideration by using the plane stress element type (with thickness option). Plane stress elements were used instead of plane strain elements. It has been reported by Schotborgh *et al.* (2005) that plane stress elements provide a safer prediction of stiffness with a possibility of 5 to 10% underestimation, while plane strain elements provide an even greater over-estimation of stiffnesses. The modelled flexure hinge has a thickness of 12.7 mm (aluminium alloy, 7075-T6) with a Young's modulus (E) of 71.7 GPa and a Poisson's ratio (v) of 0.33. A mapped meshing technique was used instead of a "smart" meshing, the latter automatically produces fine meshing at areas that high stress concentrations were most likely to occur. Mapped meshing is advantageous over "smart" meshing because mapped meshing provides better control of the distribution and size of elements in an area (see Figure 3.1). To ensure that the mesh size was fine enough especially near the smallest thickness of the hinge, a number of analyses were carried out where different mesh sizes were used. The output of each analysis was checked each time the mesh size was decreased. When a consistent output was obtained, it implied that the mesh was fine enough.

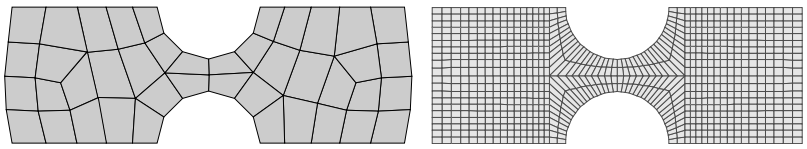

(a) "Smart" meshing (b) Mapped meshing

Figure 3.1: FEA meshing techniques

3.1.1 Boundary conditions

The accuracy of the FEA model was significantly influenced by the way the boundary conditions and forces were assigned. For example, when a point load is applied on a node, it causes a singularity on the node where the area near the node encounters a large local deformation. This will reduce the accuracy of the FEA results if displacements near the load are of interest in an analysis. To avoid inaccuracies of results associated with singularities, constraints and point loads were applied at a distance of at least $3h$ from a node where nodal displacements will be measured (see Figure 3.2).

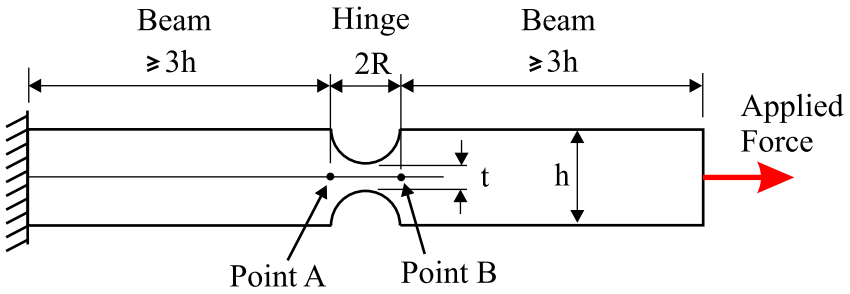

Figure 3.2: Dimensions of a FEA flexure hinge model

3.1.2 Applying forces and moments

Displacements of nodes at the left portion of flexure hinges, which have a distance of $3h$ from Point A, were constrained to be zero as shown in Figure 3.2. Forces were applied at a distance of $3h$ from Point B due to the same reason discussed in the previous section. However, analytical equations were derived to find the flexure hinge compliances at Point B (see Figure 3.3) when forces/moments were applied at this point. Although forces/moments were not applied at Point B in the FEA model, the applied forces/moments were calculated to have the equivalent loading effects as forces/moments applied at Point B. This allowed the comparison of results between the analytical and the FEA models.

Longitudinal force, F_x was applied as shown in Figure 3.4a. Since F_x was applied along the horizontal line of Point B, it provided the equivalent loading effect as F_x was directly applied on Point B.

In order to apply a pure unit force in the y-direction (transverse force, F_y) at Point B, an additional moment was applied to counter the moment effect caused by F_y. The additional moment was introduced by applying two horizontal forces, F_x in opposite direction as shown in Figure 3.4b. The value of each F_x was calculated as below,

$$M_{Fy} = F_y \times length \tag{3.1}$$

$$M_{additional} = 2F_x \times \frac{h}{2} = F_x h \tag{3.2}$$

$$\begin{aligned} M_{Fy} &= M_{additional} \\ F_y \times length &= F_x h \\ F_x &= length/h \end{aligned} \tag{3.3}$$

where F_y = 1 N (unit force), $M_{additional}$ is the additional moment and M_{Fy} is the moment caused by F_y.

Similarly, a unit moment was generated by applying two horizontal, equal forces F_x in opposite direction as shown in Figure 3.4c. Each force was set to a value of $F_x = 1/h$ to generate a unit moment, M_z applied on the model.

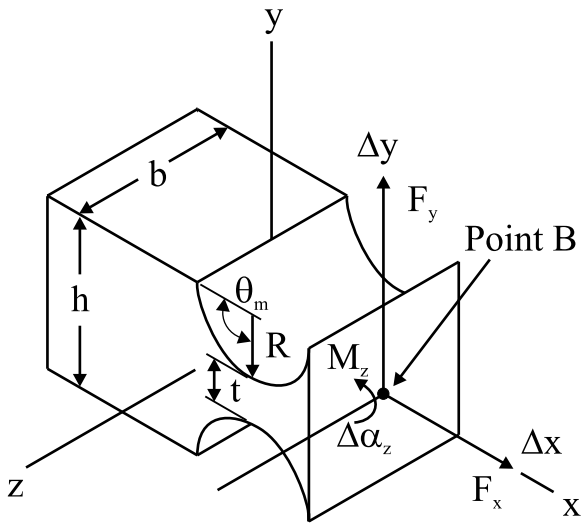

Figure 3.3: Dimensions, forces, moments and deflections of flexure hinge

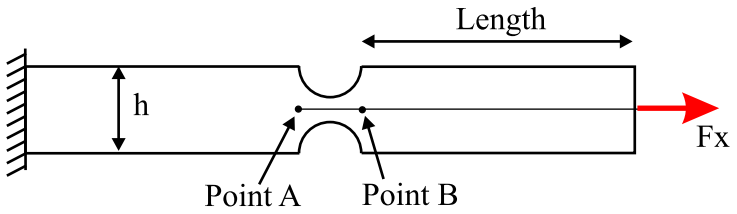

(a) Applying a unit force along the x-direction

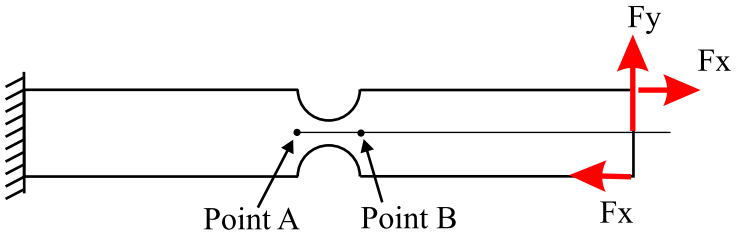

(b) Applying a pure unit force along the y-direction

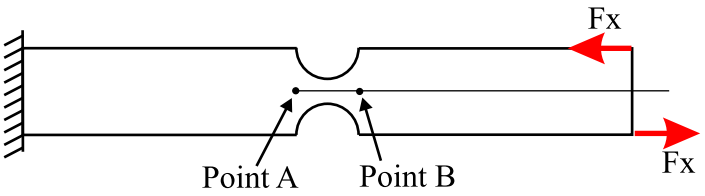

(c) Applying a unit moment about the z-direction

Figure 3.4: Method of applying forces/moments on the FEA flexure hinge model

3.1.3 Nodal deformations of FEA flexure hinge model

The FEA model in Figure 3.2 consists of two beam sections and a hinge section. Nodal deformations measured at Point B were the total deformation contributed by the left-hand side beam section as well as the hinge section. Therefore, rotations and deformations of the beam section (nodal deformations at Point A) were subtracted from the total deformation measured at Point B to obtain pure deformations caused by only the hinge.

Nodal deformations along the x-direction of flexure hinges can be easily obtained by subtracting the nodal deformations at Point A from Point B,

$$\Delta x_{hinge} = \Delta x_B - \Delta x_A \tag{3.4}$$

where Δx_A and Δx_B were nodal deformations obtained directly from FEA nodal results.

Rotational deformations at Points A and B cannot be measured directly from nodes. However, rotational motions at Points A and B can be calculated as shown in Figure 3.5. N_{A1}, N_{A2}, N_{B1} and N_{B2} are nodes at positions shown in the figure.

Ux_{nA1} and Ux_{nA2} are nodal deformations of nodes N_{A1} and N_{A2} respectively along the x-direction. Uy_{nA1} and Uy_{nA2} are deformations of nodes N_{A1} and N_{A2} respectively along the y-direction. Similar notations were assigned for Ux_{nB1}, Ux_{nB2}, Uy_{nB1} and Uy_{nB2}. Rotational motions of Points A and B were obtained as follows,

$$\Delta\alpha_A = arctan\left(\frac{Ux_{nA1} + Ux_{nA2}}{h + Uy_{nA1} - Uy_{nA2}}\right) \tag{3.5}$$

Similarly,

$$\Delta\alpha_B = arctan\left(\frac{Ux_{nB1} + Ux_{nB2}}{h + Uy_{nB1} - Uy_{nB2}}\right) \tag{3.6}$$

Therefore, rotational deformations of the hinge were obtained by subtracting rotational deformations at Point A from Point B.

$$\Delta\alpha_{hinge} = \Delta\alpha_B - \Delta\alpha_A \tag{3.7}$$

Nodal deformations caused by the beam section were subtracted from the total deformation, Δy_B at Point B in order to calculate the deformation of the hinge along the y-direction (see Figure 3.6). Δy_A and Δy_B were obtained from FEA nodal results at Points A and B respectively,

$$\Delta y_B = (\Delta y_A + 2R \times \Delta\alpha_A) + \Delta y_{hinge}$$

$$\Delta y_{hinge} = \Delta y_B - (\Delta y_A + 2R \times \Delta\alpha_A) \tag{3.8}$$

where $\Delta\alpha_A$ was obtained from Equation 3.5. $(\Delta y_A + 2R \times \Delta\alpha_A)$ is the deformation contributed by the beam section.

Compliances of flexure hinges were calculated by dividing the deformations, Δx_{hinge}, Δy_{hinge} and $\Delta\alpha_{hinge}$ by the applied forces or moment, F_x, F_y and M_z respectively.

3.2 Experimental validation of the FEA model

Three flexure hinges from each of the categories of thin ($t/R \leq 0.07$), intermediate ($0.07 < t/R \leq 0.2$) and thick ($0.2 < t/R \leq 0.8$) circular hinges were selected for experimental study to verify the accuracy of the FEA model. The three flexure hinges were manufactured via wire-EDM. The experimentally determined compliances were also compared with various analytical and empirical equations to justify that a) some of the analytical/empirical compliance equations provide better accuracies than others depending on the t/R ratios of circular flexure hinges,

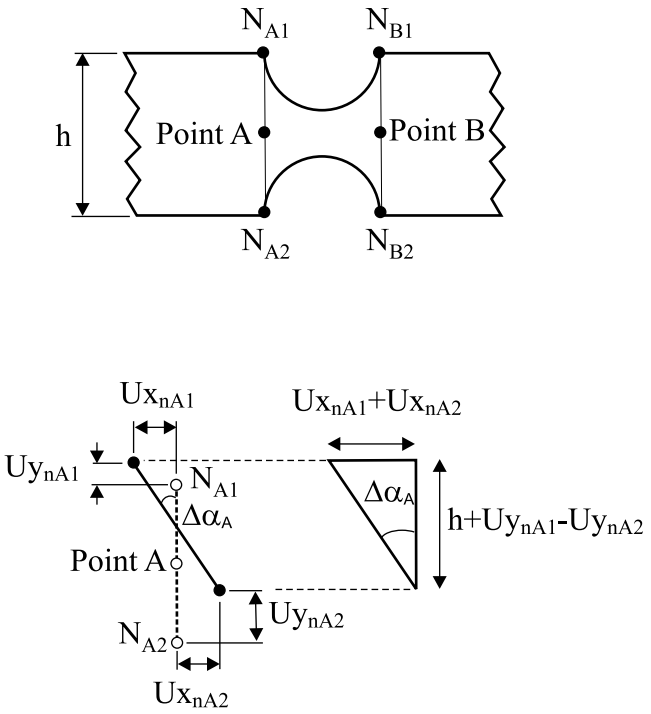

Figure 3.5: Calculation of rotational motions from nodal deformations obtained from FEA

and b) flexure hinge compliances determined using any particular method may not be accurate for a large range of t/R ratios.

The aim of this experiment was to measure the $\Delta\alpha_z$-compliance ($\Delta\alpha_z/M_z$), the Δy-compliance ($\Delta y/F_y$) and the Δx-compliance ($\Delta x/F_x$) of flexure hinges. Unfortunately, a consistent result of the Δx-compliance could not be obtained due to the limitation of the sensors and experimental setup. Flexure hinges were mounted on a plate using screws as shown in Figure 3.7. Weights were hung at the flexure hinges to apply certain forces and moments on the hinges. The stiffness along the x-direction of the flexure hinges are very high (small Δx-compliance). When weights of 10 to 200g were applied on the flexure hinges, the deformations of the flexure hinges were too small to be measured due to the limitation of the resolution of the sensors. When weights of more than 200g were applied, inconsistent deformations were measured by the sensors. The inconsistency of the measurements could be attributed to the compliances of the screws. These measured Δx-deformations could not be used to determine the Δx-compliances of the flexure hinges.

Although the Δx-compliance of the FEA model cannot be verified experimentally, the order of accuracy of the FEA determined Δx-compliance was expected to be approximately the same as the $\Delta\alpha_z$- and Δy-compliances. This assumption

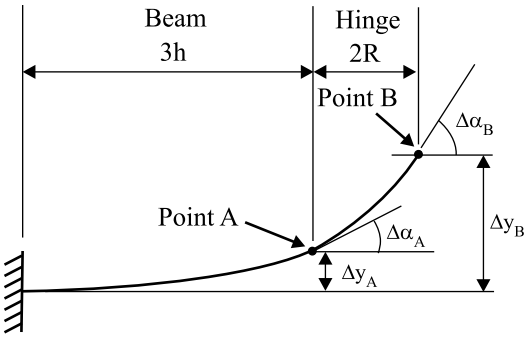

Figure 3.6: Calculation of deformation along the y-direction of the flexure hinge

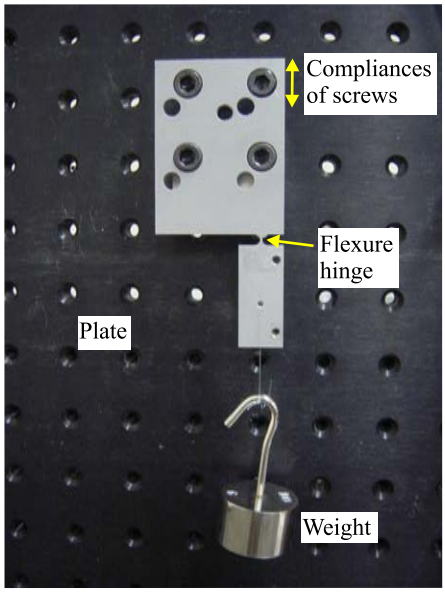

Figure 3.7: Δx-compliance measurement of flexure hinges

was made because the FEA modelling concept of determining the Δx-compliance was the same as that of the $\Delta\alpha_z$- and Δy-compliances.

3.2.1 Experimental setup

3.2.1.1 Measurement of $\Delta\alpha_z$ -compliance

The experimental setup of measuring the $\Delta\alpha_z$-compliance is shown in Figure 3.8. The experiment was setup on an anti-vibration table. Two eddy-current sensors were used to detect deformations of the hinge. These eddy-current sensors were calibrated using a Michelson laser interferometer. Details of the calibration are presented in Appendix A. The resolutions of the eddy-current sensors are 18.5 and 10.1 nm for sensor 3316 and 3317 respectively. Aluminium targets of eddy-

current sensors were mounted on the flexure hinges. Eddy-current sensors, 3316 and 3317 were mounted on translation stages. These stages have a travel range of 6 mm and a fine adjustment of 5 μm. They were used to position the two eddy-current sensors to their corresponding linear measurement ranges. Signals of the two sensors were recorded using a dSPACE DS1104 controller board via its inbuilt ADC channels. Forces were applied on the flexure hinges by hanging weights at a predetermined position as shown in Figure 3.8. Table 3.1 shows the range of weights applied on the three flexure hinges.

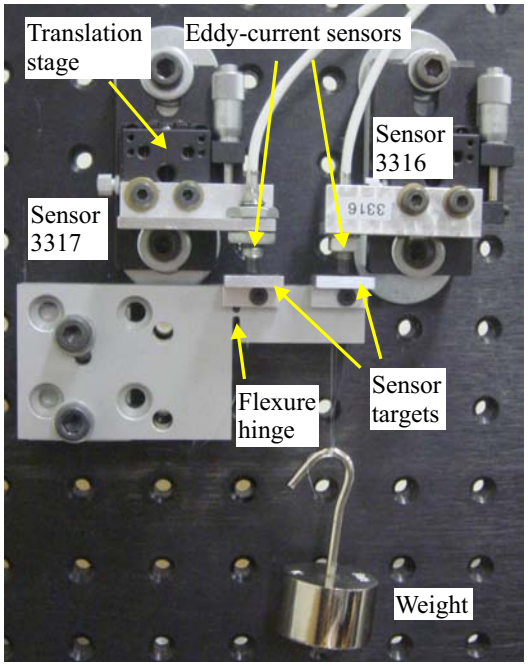

Figure 3.8: Experimental setup of the $\Delta\alpha_z$-compliance measurement of flexure hinges

Flexure hinge	t/R	Range of weight (g)
t= 0.5mm, R= 3mm	0.17	10 - 70
t= 0.7mm, R= 1.87mm	0.37	10 - 200
t= 0.84mm, R= 1.1mm	0.76	10 - 500

Table 3.1: Weights applied on the three flexure hinges to measure the $\Delta\alpha_z$-compliance

3.2.1.2 Measurement of Δy-compliance

The experimental setup of measuring the Δy-compliance is shown in Figure 3.9. This experiment was setup similar to Section 3.2.1.1 except that a fibre-optic sensor was used instead of the two eddy-current sensors. This is because the fibre-optic sensor has smaller resolution than the eddy-current sensors which is more suited for measuring the small Δy-deformations of flexure hinges. The fibre-optic sensor was calibrated using the Michelson laser interferometer (see Appendix A for details). The resolution of the fibre-optic sensor is 3.5 nm. The fibre-optic sensor was mounted on a NanoFlex$^{\mathrm{TM}}$ translation stage which has a travel range of 5 mm and a resolution of 50 nm. The translation stage was used to position the fibre-optic sensor to its measurement range. Forces were applied on the flexure hinge by hanging weights at a predetermined position shown in Figure 3.9. Table 3.2 shows the range of weights applied on the three flexure hinges.

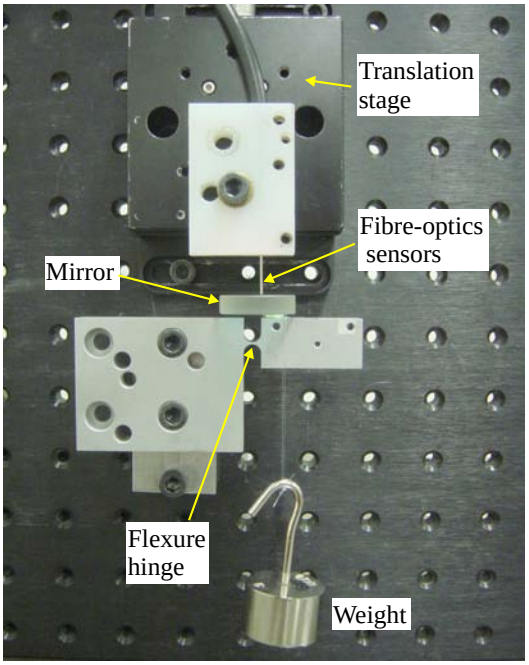

Figure 3.9: Experimental setup of the Δy-compliance measurement of flexure hinges

Flexure hinge	t/R	Range of weight (g)
t= 0.5mm, R= 3mm	0.17	10 - 200
t= 0.7mm, R= 1.87mm	0.37	100 - 500
t= 0.84mm, R= 1.1mm	0.76	100 - 500

Table 3.2: Weights applied on the three flexure hinges to measure the Δy-compliance

3.2.2 Experimentally determined flexure hinge compliances

3.2.2.1 $\Delta\alpha_z$-compliance

The $\Delta\alpha_z$-deformation of a flexure hinge can be calculated easily from deformations detected by sensors 3316 and 3317. Figure 3.10 shows the schematic of the experimental setup and dimensions.

The rotational angle of the hinge is,

$$\Delta\alpha_z = \arctan\left(\frac{d_1 - d_2}{L_1 - L_2}\right) \tag{3.9}$$

where d_1 and d_2 are the displacements measured by the sensors.

Therefore, the $\Delta\alpha$- compliance ($\Delta\alpha_z/M_z$) is calculated as,

$$\frac{\Delta\alpha_z}{M_z} = \frac{\Delta\alpha_z}{F_1\left(L_1 + R\right)} \tag{3.10}$$

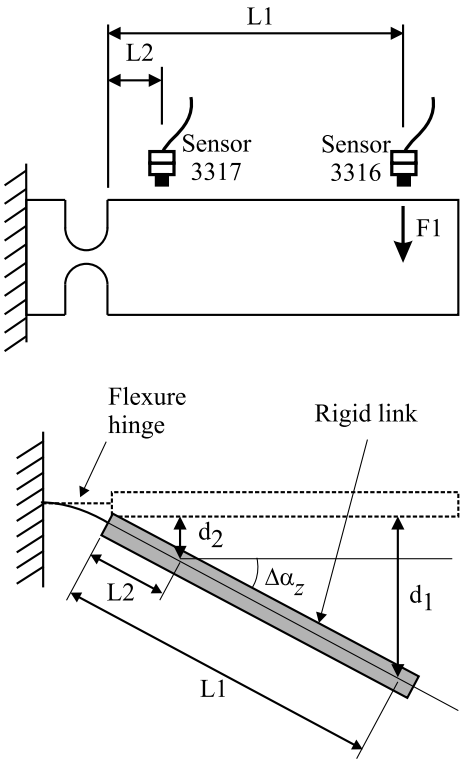

Figure 3.10: Schematic of the experimental setup

3.2.2.2 Δy-compliance

The overall deformation measured by the fibre-optic sensor consists of a deformation component caused by a force, $F_y = F_2$ and a deformation component caused by a moment, $M_{z2} = F_2 L_2$ (see Figure 3.11). In order to calculate the Δy-deformation and compliance which are only caused by F_y, the deformation caused by M_{z2} is required to be subtracted from the measured results.
Rotational deformation caused by M_{z2} is,

$$\Delta\alpha_{z,M_{z2}} = \frac{\Delta\alpha_z}{M_z} \cdot M_{z2} \tag{3.11}$$

where $\dfrac{\Delta\alpha_z}{M_z}$ is determined from Equation 3.10.
Δy-deformation caused by M_{z2} is,

$$\Delta y_{M_{z2}} = \Delta\alpha_{z,M_{z2}} \cdot R \tag{3.12}$$

Thus, the Δy-deformation caused by F_y is,

$$\Delta y = \Delta y_{fibre-optics} - \Delta y_{M_{z2}} \tag{3.13}$$

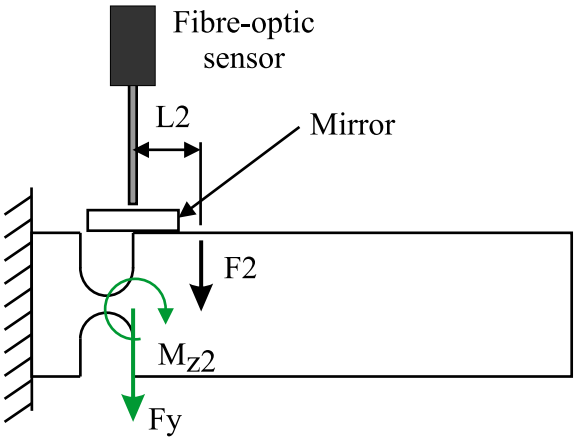

Figure 3.11: Equivalent forces/moment on a flexure hinge

The Δy-compliance ($\Delta y/F_y$) of the hinge is then calculated by dividing Equation 3.13 with F_y.

3.2.3 Experimental results and comparisons

Table 3.3 shows the average experimental results of compliances each obtained from 25 sets of measurement data for the $\Delta\alpha_z$- and Δy-compliances. The table also illustrates the comparison of compliances between FEA and experimental results. The FEA determined $\Delta\alpha_z$-compliances were within 3% of the experimental results while the Δy-compliances were within 6% of the experimental compliances. These results indicated that the developed FEA model was defined with appropriate boundary conditions and mesh sizes, and the model was capable of providing good accuracies of compliance results for flexure hinges with different t/R ratios. The comparison of results also confirmed that the FEA model can be used as a benchmark for comparisons with other analytical results without much loss of accuracy.

In order to further justify the accuracy of the FEA results presented in this thesis, the FEA results were also compared to the experimental results of Smith *et al.* (1997). Smith *et al.* measured only the $\Delta\alpha_z$-compliances of three flexure hinges with t/R= 0.125, 0.246 and 0.403 respectively. Table 3.4 shows the comparison of compliances between the FEA results (this thesis) and the experimental results of Smith *et al.* (1997). The maximum difference between the FEA and experimental results is 6.2%. These results again confirm that the FEA model is capable of providing good accuracies of compliance results of flexure hinges with different t/R ratios and the FEA model can be used as a benchmark for comparisons with other analytical results without much loss of accuracy.

Flexure hinge	t/R	$\Delta\alpha_z/M_z$(rad/Nm)			$\Delta y/F_y(\mu$m/N)		
		FEA	Exp.	% diff.	FEA	Exp.	% diff.
t= 0.5mm, R= 3mm	0.167	0.1574	0.1590	-1.0	1.5188	1.4774	2.8
t= 0.7mm, R= 1.87mm	0.374	0.0563	0.0556	1.3	0.2275	0.2181	4.3
t= 0.84mm, R= 1.1mm	0.764	0.0290	0.0283	2.6	0.0470	0.0442	6.2

Table 3.3: A comparison of FEA results to experimental results (this thesis)

Flexure hinge	t/R	$\Delta\alpha_z/M_z$(rad/Nm)		
		FEA	Exp. (Smith *et al.*, 1997)	% diff.
t= 1.19mm, R= 9.53mm	0.125	0.0311	0.0293	6.2
t= 2.34mm, R= 9.53mm	0.246	0.0060	0.0059	3.0
t= 3.38mm, R= 9.53mm	0.403	0.0018	0.0018	-0.5

Table 3.4: A comparison of FEA results to the experimental results of Smith *et al.* (1997)

The results of previously derived analytical and empirical compliance equations were also compared to the experimental results presented in this thesis. Tables 3.5 to 3.7 show the comparison of various analytical and empirical compliances to the experimentally determined compliances of this thesis. It was observed that most of the analytical or empirical compliance equations had small differences when compared to experimental results for t/R= 0.167 (Table 3.5). However, the differences of equations of Paros and Weisbord (1965) (both full and simplified), Wu and Zhou (2002), Lobontiu (2003) and Tseytlin (2002) increase when t/R= 0.764 (Table 3.7). Equations of Smith *et al.* (1987), Schotborgh *et al.* (2005) and Zhang and Fasse (2001) have small differences (approximately 5%) for all the three flexure hinges with t/R= 0.167, 0.374 and 0.764 respectively. The results of the comparisons show that a) some of the analytical/empirical compliance equations provide better accuracies than others depending on the t/R ratio of circular flexure hinges, and b) flexure hinge compliances determined using any particular method may not be accurate for a large range of t/R ratios. Therefore, a proper scheme for se-

t/R= 0.167, $[\Delta\alpha_z/M_z]_{exp}$= 0.159 rad/Nm, $[\Delta y/F_y]_{exp}$= 1.477 μm/N

Analytical/Empirical	$\Delta\alpha_z/M_Z$ (rad/Nm)	% diff.	$\Delta y/F_y$ (μm/N)		% diff.
PW (Full), Wu and Zhou (2002)	0.1482	-6.4	no shear compliance with shear compliance	1.3952 1.4114	-5.2 -4.1
PW (Simplified)	0.1515	-4.3	no shear compliance with shear compliance	1.3633 1.3882	-7.3 -6.3
Lobontiu (2003)	0.1482	-6.4	no shear compliance with shear compliance	1.3952 1.4195	-5.2 -3.5
Tseytlin (2002)	0.1612	1.8	NA		NA
Smith *et al.* (1987)	0.1639	3.5	NA		NA
Schotborgh *et al.* (2005)	0.1549	-2.2	NA		NA
Zhang and Fasse (2001)	0.1503	-5.1	NA		NA

Table 3.5: Comparisons of various compliance equations to experimental results - First flexure hinge, t= 0.5 mm, R= 3 mm. Paros and Weisbord (1965) is referred as PW

lecting the most suitable and accurate compliance equation based on the t/R ratio is required.

3.3 A scheme for selecting flexure hinge compliance equations

The results of comparisons between experimental and various analytical/ empirical compliances in Section 3.2.3 show that some of the analytical/empirical compliance equations provide better accuracies than others depending on the t/R ratio of circular flexure hinges. In order to assist designers in selecting the most suitable compliance analytical and empirical equations, a review of the accuracies and limitations of various previously derived equations at different t/R ratios is presented based on their differences when compared to the FEA results obtained in this thesis. Suggestions of the most appropriate equation to be used at any particular t/R range are provided in this chapter. Throughout the review process, it was also found that there was no accurate equation (within 5% difference when compared to FEA results) to predict the Δx- and Δy-compliances of circular flexure hinges for a wide t/R range ($0.05 \leq t/R \leq 0.8$). Therefore, general empirical equations

t/R= 0.374, $[\Delta\alpha_z/M_z]_{exp}$= 0.0556 rad/Nm, $[\Delta y/F_y]_{exp}$= 0.2181 μm/N

Analytical/Empirical	$\Delta\alpha_z/M_Z$ (rad/Nm)	% diff.	$\Delta y/F_y$ (μm/N)		% diff.
PW (Full), Wu and Zhou (2002)	0.0491	-11.3	no shear compliance with shear compliance	0.1864 0.1957	-14.2 -9.9
PW (Simplified)	0.0516	-6.8	no shear compliance with shear compliance	0.1803 0.1878	-17.0 -13.5
Lobontiu (2003)	0.0491	-11.3	no shear compliance with shear compliance	0.1864 0.2004	-14.2 -7.7
Tseytlin (2002)	0.0535	-3.4	NA		NA
Smith *et al.* (1987)	0.0540	-2.4	NA		NA
Schotborgh *et al.* (2005)	0.0558	0.9	NA		NA
Zhang and Fasse (2001)	0.0539	-2.7	NA		NA

Table 3.6: Comparisons of various compliance equations to experimental results - Second flexure hinge, t= 0.7 mm, R= 1.87 mm. Paros and Weisbord (1965) is referred as PW

t/R= 0.764, $[\Delta\alpha_z/M_z]_{exp}$= 0.0283 rad/Nm, $[\Delta y/F_y]_{exp}$= 0.0442 μm/N

Analytical/Empirical	$\Delta\alpha_z/M_Z$ (rad/Nm)	% diff.	$\Delta y/F_y$ (μm/N)		% diff.
PW (Full), Wu and Zhou (2002)	0.0227	-19.4	no shear compliance with shear compliance	0.0312 0.0366	-29.2 -16.9
PW (Simplified)	0.0251	-10.9	no shear compliance with shear compliance	0.0303 0.0333	-31.1 -24.4
Lobontiu (2003)	0.0227	-19.4	no shear compliance with shear compliance	0.0312 0.0394	-29.2 -10.7
Tseytlin (2002)	0.0318	13.2	NA		NA
Smith *et al.* (1987)	0.0291	3.4	NA		NA
Schotborgh *et al.* (2005)	0.0296	5.1	NA		NA
Zhang and Fasse (2001)	0.0281	-0.1	NA		NA

Table 3.7: Comparisons of various compliance equations to experimental results - Third flexure hinge, t= 0.84 mm, R= 1.1 mm. Paros and Weisbord (1965) is referred as PW

were developed based on FEA results to estimate the Δx- and Δy-compliances of circular flexure hinges for $0.05 \leq t/R \leq 0.8$.

3.3.1 A comparison of compliance results with FEA

3.3.1.1 $\Delta\alpha_z$-compliance equations

Compliances, $\Delta\alpha_z/M_z$ of different circular flexure hinges (with various t and R values), where t/R in a range 0.05 to 0.8, were calculated using hinge equations of a) Paros and Weisbord (1965) (full), b) Paros and Weisbord (1965) (simplified), c) Lobontiu (2003), d) Wu and Zhou (2002), e) Tseytlin (2002), f) Smith *et al.* (1987) (empirical), g) Schotborgh *et al.* (2005) (empirical) and h) Zhang and Fasse (2001) (empirical). These analytical and empirical equations are presented in Appendix C for references. Their results were compared with that of the FEA model developed in Section 3.1.3. Differences of the comparison were plotted in Figure 3.12. From the figure, it is noted that,

- equations of Paros and Weisbord (full), Lobontiu, and Wu and Zhou were derived using a similar method (that was based on the integration of the linear differential equation of a beam); thus their equations have the same accuracy when compared to FEA results. The differences of their results when compared to the FEA results increase over the t/R range. Differences are less than 5% when $0.05 \leq t/R < 0.15$. Differences increased to more than 5% but less than 10% when $0.15 \leq t/R < 0.3$. When $0.3 \leq t/R \leq 0.8$, differences increase from 10% to 22%;

- Paros and Weisbord's (simplified) results are within 5% of the FEA results for $0.05 \leq t/R \leq 0.2$. Differences increase up to 10% when $t/R = 0.5$ and 13% when $t/R = 0.8$;

- Tseytlin's results are within 6% of the FEA results for $t/R \leq 0.23$ and $0.35 \leq t/R < 0.65$. The differences are more than 6% when $0.23 < t/R < 0.35$. When $t/R = 0.25$, the difference is 11.2%. Generally, the differences of the results are within 10% approximately for the entire t/R range. Tseytlin's analytical results are different from his experimental and FEA results by about 10% (Tseytlin, 2002), which are in agreement with the results of comparison presented in this section;

- Smith *et al.*'s (empirical) results are within 4% of the FEA results for $0.20 \leq t/R \leq 0.8$. Their results have large differences for $t/R < 0.2$;

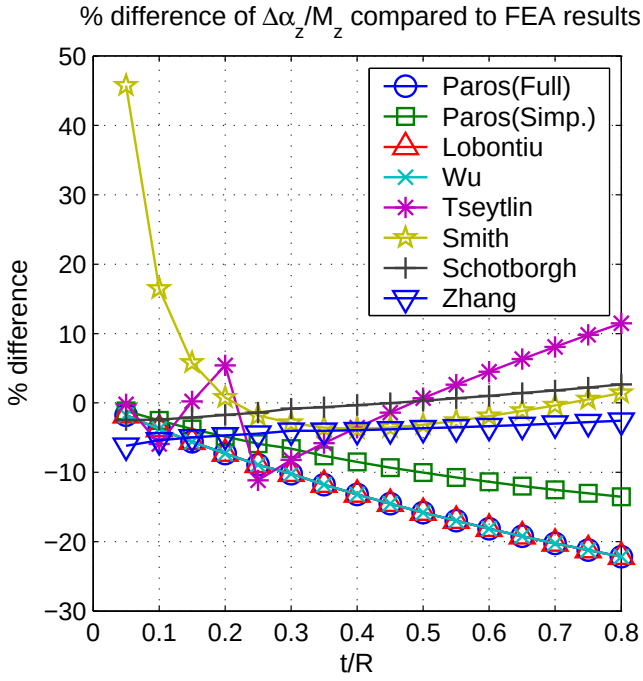

Figure 3.12: Differences of various compliance equations, $\Delta\alpha_z/M_z$ compared to FEA results

- Schotborgh *et al.*'s results are within 3% of the FEA results for the entire range of $0.05 \leq t/R \leq 0.8$ range; and
- Zhang and Fasse's equation is within 8% of the FEA results for $0.05 \leq t/R \leq 0.2$. The differences become consistent (within 5%) for $0.2 < t/R \leq 0.8$.

3.3.1.2 Δx- and Δy-compliance equations

Differences of $\Delta x/F_x$ and $\Delta y/F_y$, calculated using design equations of a) Paros and Weisbord (1965) (full), b) Paros and Weisbord (1965) (simplified), c) Lobontiu (2003), d) Wu and Zhou (2002) and e) Schotborgh *et al.* (2005) (empirical), were plotted in Figure 3.13 and 3.14 respectively.
For $\Delta x/F_x$,

- Paros and Weisbord (full), Lobontiu, and Wu and Zhou achieve the same results. Their results are within 6% of the FEA results;
- results of Paros and Weisbord (simplified) are not as close as that of Paros and Weisbord (full), Lobontiu, and Wu and Zhou when compared to the FEA results. Paros and Weisbord's (simplified) results have a minimum difference of 6.6%, and a maximum difference of 49%. The large differences of Paros

and Weisbord's equation at high t/R ratios are expected due to the assumption, $t \ll 2R$ used to simplify their equation. At high t/R ratios, the assumption is violated; therefore the accuracy of the simplified equation is reduced; and

- Schotborgh *et al*. are not as close as that of Paros and Weisbord (full), Lobontiu, and Wu and Zhou when compared to the FEA results. Schotborgh *et al*.'s results have a minimum difference of 16%, and a maximum difference of 85% respectively. The reason of the large differences of Schotborgh's equation compared to that of other research groups will be discussed later in this section.

For $\Delta y/F_y$ (without shear compliance, SC),

- results of Paros and Weisbord (full), Lobontiu, and Wu and Zhou, without considering shear compliances (SC), are the same. Their differences are within 10% for $0.05 \leq t/R \leq 0.2$. Differences increase up to 30% when $t/R = 0.65$. When $t/R = 0.8$, the difference is approximately 38%; and
- Paros and Weisbord's (simplified) results are within 10% when $0.05 \leq t/R \leq 0.17$. Differences increase to 31% when $t/R = 0.65$. When $t/R = 0.8$, the difference is approximately 39%.

For $\Delta y/F_y$ (with shear compliance, SC),

- Lobontiu's results are the closest to the FEA results compared to that of others. The results are within 5% difference for $0.05 \leq t/R \leq 0.1$. The differences increase to within 10% for $0.1 < t/R \leq 0.3$ and to within 18% for $0.3 < t/R \leq 0.8$;
- results of Paros and Weisbord's (full) and Wu and Zhou are the same. Their results are within 5% difference for $0.05 \leq t/R \leq 0.1$. The differences increase to within 10% for $0.1 < t/R \leq 0.25$ and to within 22% for $0.25 < t/R \leq 0.8$;
- Paros and Weisbord's (simplified) results are within 5% difference for $0.05 \leq t/R < 0.1$. The differences increase to within 10% for $0.1 \leq t/R \leq 0.17$. The maximum difference is 29% when $t/R = 0.8$;
- Schotborgh *et al*.'s compliance results ($\Delta y/F_y$) do not involve shear compliance. Their results have the largest difference compared to the others. The minimum difference is 70% and the maximum difference is 98%. The reason of the large differences of Schotborgh's equation compared to that of other research groups will be discussed later in this section.

Generally, all compliance equations, $\Delta y/F_y$ (except Schotborgh *et al.*'s) are closer to the FEA results when shear compliances are considered.

3.3.1.2.1 Discussion of the Δx- and Δy-compliance equations of Schotborgh *et al.* (2005) Schotborgh *et al.*'s compliance equations in the x- and y-directions ($\Delta x/F_x$ and $\Delta y/F_y$) have large differences compared to other research groups. Schotborgh *et al.* developed the compliance equations using a FEA flexure hinge model with a larger height than that used in this thesis (see Figure 3.15a). Schotborgh *et al.*'s compliances were obtained using a spring model (as shown in Figure 3.15b) which consists of two springs that are connected in series (as told via a personal communication with Schotborgh). k_{hinge} and k_{beam} are the stiffnesses of the hinge and beam respectively. k_{beam} is calculated using the beam equation below,

$$k_{beam} = \frac{EA}{l} \tag{3.14}$$

where E is the Young's modulus, A is the cross-sectional area of the beam and l is the length of the beam.

Equation 3.15 below is used to calculate the stiffness of the hinge,

$$\left(\frac{1}{k_{hinge}}\right)^{-1} = \left(\frac{1}{k_{total}} - \frac{1}{k_{beam}}\right)^{-1} \tag{3.15}$$

where k_{total} is the total stiffness calculated from the FEA model. For example, to calculate the stiffness of a hinge along the x-direction, a unit displacement U_x was applied at all the nodes at the end of the beam as shown in Figure 3.15a. The sum of the reaction forces $F_{x,total}$ of the nodes were calculated by ANSYS. k_{total} along the x-direction was then calculated by dividing $F_{x,total}$ by U_x.

It was found by the author and Schotborgh (via personal communication) that there were inconsistencies with this modelling technique. It was found that the stiffness of the hinge k_{hinge} varies with the height of the FEA hinge model (see Figure 3.16). These results were unexpected because k_{hinge} should remain the same for the same hinge dimensions (t and R) and material properties. The inconsistency in the FEA modelling technique may explain the differences of Schotborgh *et al.*'s results with the others. Nevertheless, the investigation of the change of k_{hinge} with the change of the model height in the FEA modelling technique is beyond the scope of this thesis. This modelling inconsistency is recommended to be investigated in the future.

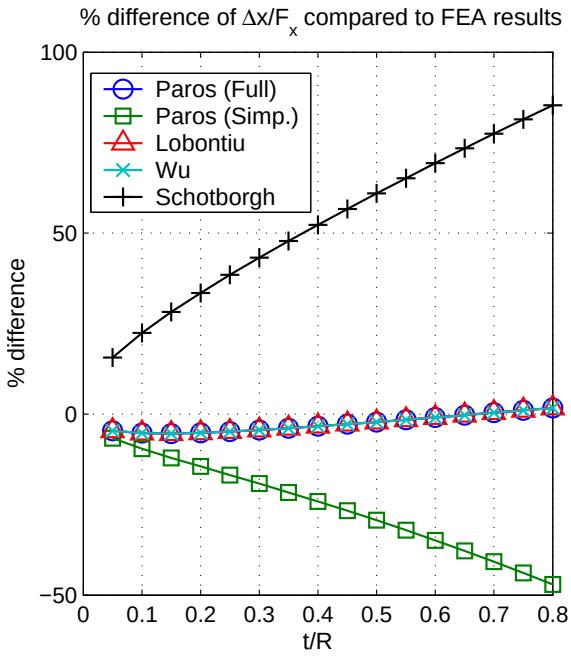

(a) Including results of Schotborgh *et al.* (2005)

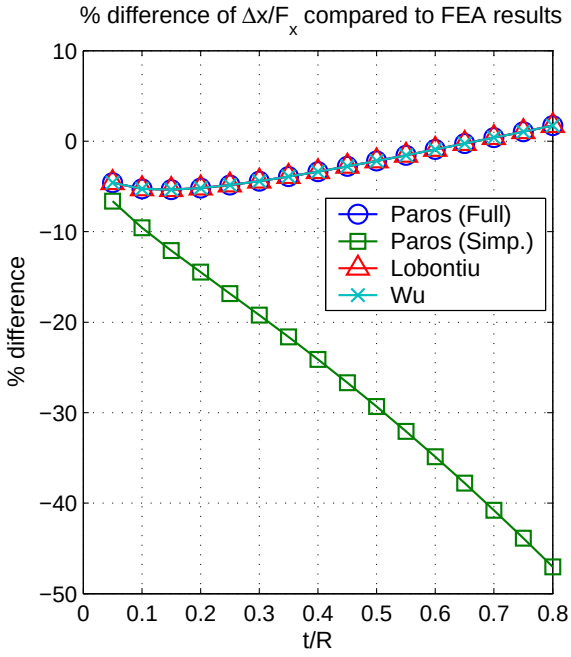

(b) Excluding results of Schotborgh *et al.* (2005)

Figure 3.13: Differences of various compliance equations, $\Delta x/F_x$ compared to FEA results

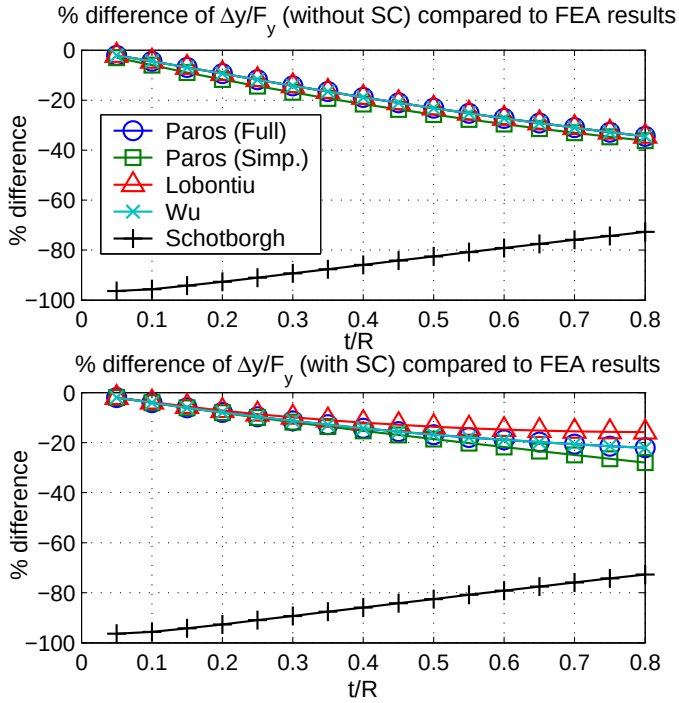

(a) Including results of Schotborgh *et al.* (2005)

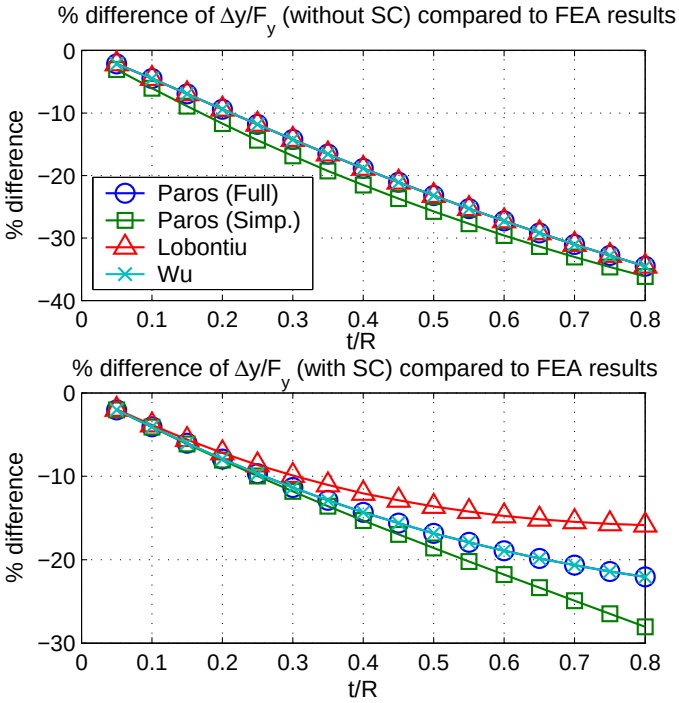

(b) Excluding results of Schotborgh *et al.* (2005)

Figure 3.14: Differences of various compliance equations, $\Delta y/F_y$ compared to FEA results

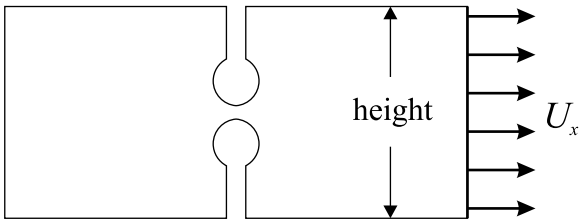

(a) FEA hinge model

(b) Spring model of flexure hinges

Figure 3.15: Flexure hinge models of Schotborgh *et al.* (2005)

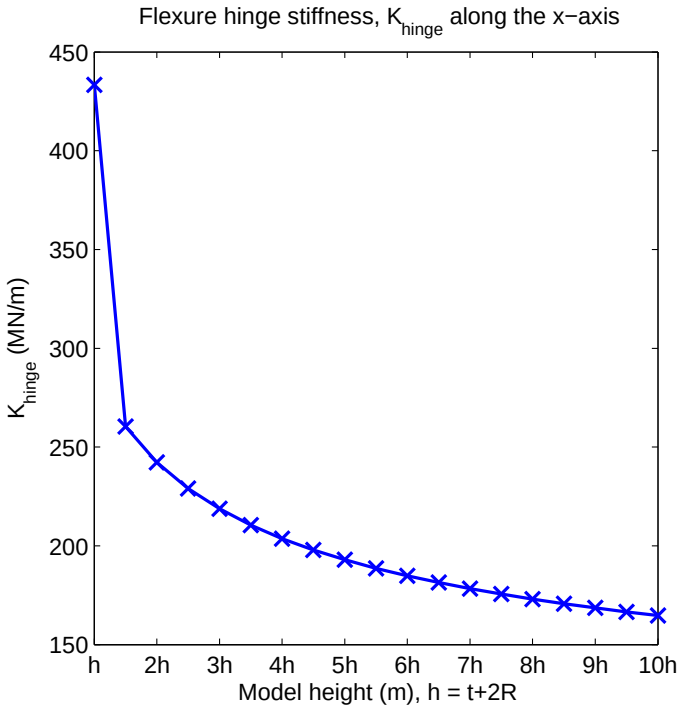

Figure 3.16: The change of k_{hinge} with the height of the FEA model of Schotborgh *et al.* (2005)

3.3.2 Empirical Δx- and Δy-compliance equations

It was observed that there were no accurate design equations (within 5% difference) to estimate the Δx-compliance for $0.1 < t/R < 0.25$ and the Δy-compliance for $t/R > 0.15$. Therefore, general empirical equations in stiffness form, named K_x and K_y were developed based on FEA results to estimate stiffness in both the x and y directions for a wide range of t/R ratios ($0.05 \leq t/R \leq 0.8$). The empirical Δx- and Δy-compliance equations were then found by inversing K_x and K_y. FEA models with various t/R ratios, which were set from 0.05 to 0.8 with an increment of 0.01, were generated in ANSYS. Unit forces, F_x and F_y were applied on each model and the corresponding nodal deformations, Δx and Δy were measured. Polynomial functions with 3rd, 4th, 5th and 6th order were fitted through the data points to obtain empirical stiffness equations. The results of these four empirical equations were compared with FEA results and their differences were plotted in Figure 3.17 and 3.18. 5th and 6th order polynomial functions were chosen for K_x and K_y respectively in order to keep the differences as small as possible. Maximum differences of the two polynomial functions occur when $t/R = 0.05$, which are 1.1% and 2.7% for K_x and K_y respectively. Both empirical equations, $\Delta x/F_x$ and $\Delta y/F_y$ (the inverse of K_x and K_y respectively) are shown in Equations 3.17 and 3.19,

$$K_x = Eb\left[\sum_{k=0}^{n} c_k \left(\frac{t}{R}\right)^k\right] \tag{3.16}$$

$$[\Delta x/F_x]_{this\,thesis} = K_x^{-1} = \left\{Eb\left[\sum_{k=0}^{n} c_k \left(\frac{t}{R}\right)^k\right]\right\}^{-1} \tag{3.17}$$

$$K_y = Eb\left[\sum_{k=0}^{n} c_k \left(\frac{t}{R}\right)^k\right] \tag{3.18}$$

$$[\Delta y/F_y]_{this\,thesis} = K_y^{-1} = \left\{Eb\left[\sum_{k=0}^{n} c_k \left(\frac{t}{R}\right)^k\right]\right\}^{-1} \tag{3.19}$$

where c_k are the coefficients of polynomial functions, n is the order of a polynomial function. Table 3.8 exhibits coefficients of these equations.

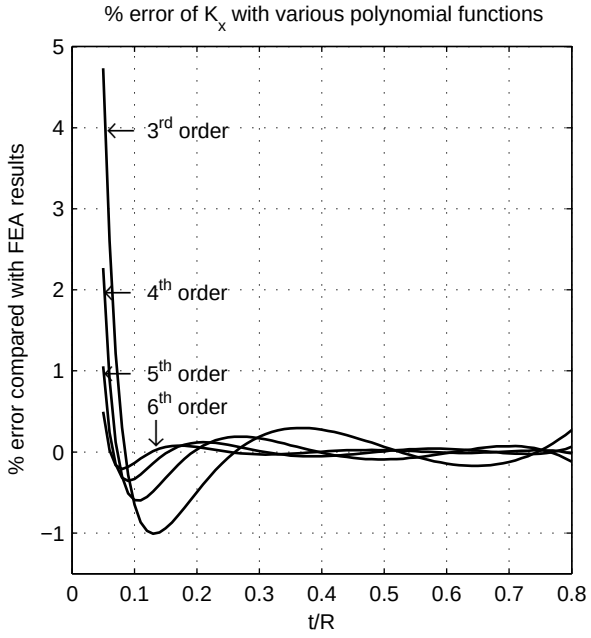

Figure 3.17: Differences of empirical equations, K_x

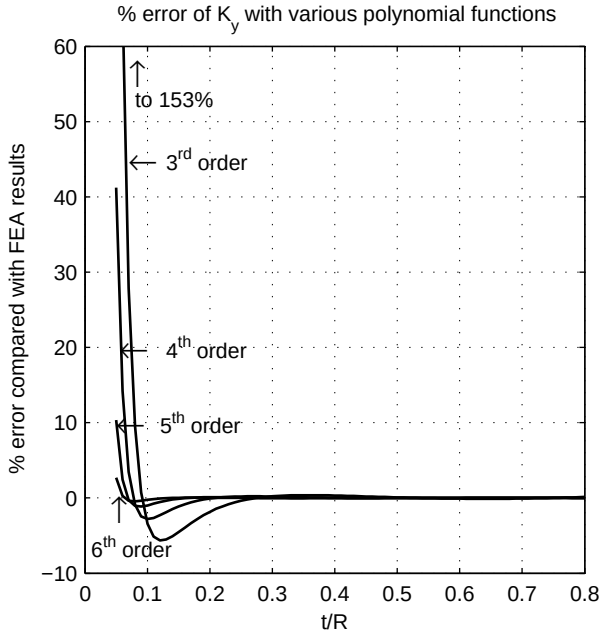

Figure 3.18: Differences of empirical equations, K_y

Finally, Table 3.9 summarises the suggested compliance equations to be used for any particular t/R range with maximum differences of less than 5% based on Figures 3.12, 3.13 and 3.14. The minimum, maximum and average differences of the compliance equations are also presented.

Coefficients	K_x, 5th order	K_y, 6th order
c_0	0.036343	1.92×10^{-5}
c_1	0.98683	-0.00083463
c_2	-1.5469	0.021734
c_3	3.1152	0.064783
c_4	-3.0831	-0.088075
c_5	1.2031	0.062278
c_6	-	-0.018781

Table 3.8: Coefficients of polynomial functions for K_x and K_y

Research Group	$\Delta\alpha_z/M_z$ t/R range	% difference min.	max.	ave.	$\Delta y/F_y$ (with SC) t/R range	% difference min.	max.	ave.	$\Delta x/F_x$ t/R range	% difference min.	max.	ave.
PW (full)	$0.05 \leq t/R < 0.1$	1.8	5.0	3.5	$0.05 \leq t/R \leq 0.1$	2	4	3.1	$0.25 \leq t/R \leq 0.8$	0.3	4.9	2.3
PW (simpl.)	$0.05 \leq t/R \leq 0.2$	1.2	4.9	3.1	$0.05 \leq t/R \leq 0.1$	3	4.7	3.7	Not recommended			
Lobontiu	$0.05 \leq t/R < 0.1$	1.8	5.0	3.5	$0.05 \leq t/R \leq 0.1$	2	3.9	2.9	$0.25 \leq t/R \leq 0.8$	0.3	4.9	2.3
Wu and Zhou	$0.05 \leq t/R < 0.1$	1.8	5.0	3.5	$0.05 \leq t/R \leq 0.1$	2	4	3.1	$0.25 \leq t/R \leq 0.8$	0.3	4.9	2.3
Tseytlin	$0.4 \leq t/R \leq 0.6$	0.7	4.5	2.5	NA	NA	NA	NA	NA	NA	NA	NA
Smith	$0.2 \leq t/R \leq 0.8$	0.3	3.7	2.1	NA	NA	NA	NA	NA	NA	NA	NA
Schotborgh	$0.05 \leq t/R \leq 0.8$	0.03	2.7	1.4	NA	NA	NA	NA	NA	NA	NA	NA
This thesis	NA	NA	NA	NA	$0.05 \leq t/R \leq 0.8$	0	2.7	0.07	$0.05 \leq t/R \leq 0.8$	0	1.1	0.08

Table 3.9: Suggested compliance/stiffness equations for a particular t/R range of circular flexure hinges. PW refers to Paros and Weisbord

3.4 Concluding remarks

This chapter presents a review of the accuracies and limitations of various flexure hinge compliance equations by comparing the results of the equations to that of FEA models. Based on the result of comparisons, a scheme for selecting the most accurate and appropriate flexure hinge compliance equation was developed. Throughout the review process, it was also found that there was no accurate equation (within 5% difference when compared to FEA results) to predict the Δx- and Δy-compliances of circular flexure hinges for a wide t/R range ($0.05 \leq t/R \leq 0.8$). Therefore, general empirical equations were developed based on FEA results to estimate the Δx- and Δy-compliances of circular flexure hinges for $0.05 \leq t/R \leq 0.8$.

The FEA model presented in this chapter was experimentally verified and the results show that the FEA model provided good estimation of hinge compliances (within 3% difference for $\Delta\alpha_z$-compliance and 6% difference for Δy-compliance) for flexure hinges with $0.05 \leq t/R \leq 0.8$. The FEA results were also compared to the experimental results of Smith *et al.* (1997) and the maximum difference was only 6.2%. Therefore, the FEA model was appropriate to be used a) as a benchmark for comparisons with various compliance equations during the review process, and b) to develop the empirical Δx- and Δy-compliance equations of flexure hinges.

CHAPTER 4

Kinematic Modelling of Micro-motion Stages using the PRBM and Loop-closure Theory

In the past, compliant micro-motion stages were commonly modelled using the Pseudo-Rigid-Body-Model (PRBM) (Scire and Teague, 1978; Furukawa *et al.*, 1995; Yang *et al.*, 1996). This method commonly models flexure hinges as purely rotational joints with rotational stiffnesses and the thick sections joining the flexure hinges as rigid-links. Therefore conventional rigid-link mechanism theory can be used to derive the kinematic model. However, the PRBM which excludes the modelling of the Δx- and Δy-displacements of flexure hinges may lead to modelling inaccuracy of compliant mechanisms. In order to compare the modelling accuracy of the PRBM method (which excludes the Δx- or Δy-displacements) with the kinetostatic model developed in this thesis, kinematic models of a four-bar compliant mechanism and a 3-RRR compliant micro-motion stage were derived using the PRBM and the loop-closure theory in this chapter. The results of the kinematic models derived using the PRBM method will be compared with the kinetostatic, FEA and experimental results presented in Chapters 5, 6 and 7 respectively.

4.1 PRBM and loop-closure theory

The derivation of the kinematic model of a 3-RRR micro-motion stage using the PRBM method and the loop-closure theory has been shown in the author's previous work (Yong *et al.*, 2003). This section presents the updated kinematic modelling of a four-bar compliant mechanism and a 3-RRR micro-motion stage based

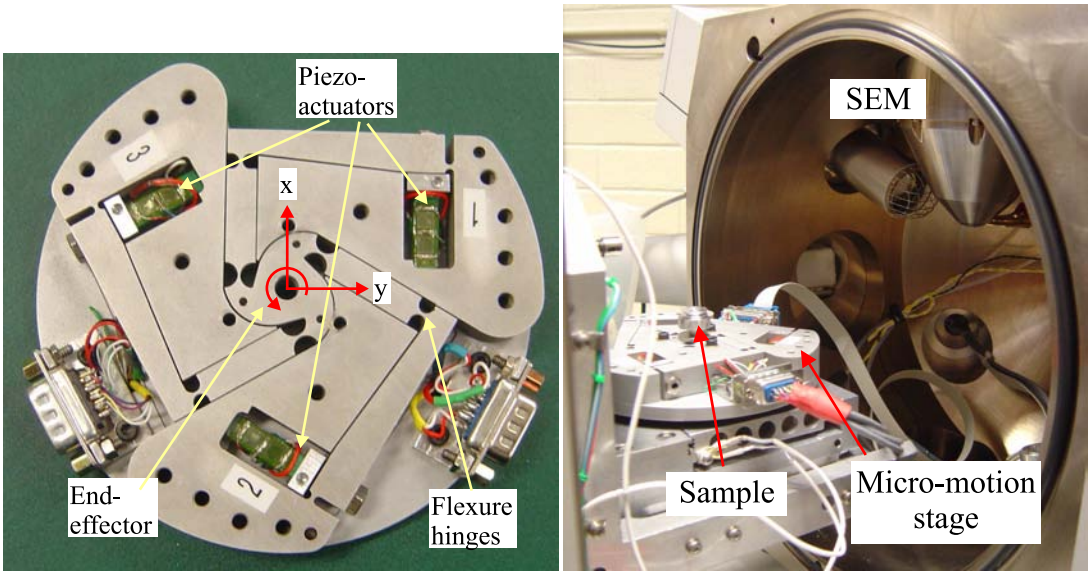

(a) 3-RRR micro-motion stage

(b) Micro-motion stage and the scanning-electron-microscope

Figure 4.1: Micro-motion system

on the same method and theory. The 3-RRR micro-motion stage studied in this thesis was designed to manoeuvre samples in a scanning-electron-microscope (SEM). Figure 4.1 shows the micro-motion stage and the microscope.

4.1.1 PRBM of compliant micro-motion stages

As mentioned before, the PRBM commonly models circular flexure hinges as revolute joints with rotational stiffness. The PRBM of circular flexure hinges is shown in Figure 4.2. Figure 4.3 shows the PRBM of the four-bar compliant mechanism and the SEM 3-RRR micro-motion stage.

For the four-bar compliant mechanism, flexure hinges are labelled as A, B, C and D. $\Delta\alpha_A$, $\Delta\alpha_B$, $\Delta\alpha_C$ and $\Delta\alpha_D$ represent the change of the angular displacements of the flexure hinges.

For the 3-RRR micro-motion stage, flexure hinges are labelled as A_i, B_i and C_i, where i= 1, 2 and 3. $\Delta\alpha_{Ai}$, $\Delta\alpha_{Bi}$ and $\Delta\alpha_{Ci}$ represent the change of the angular displacements of the flexure hinges.

4.1.2 Loop-closure theory

Loop-closure theory incorporates the complex number method to model the kinematics of mechanisms. A loop equation was generated for each closed-loop in the

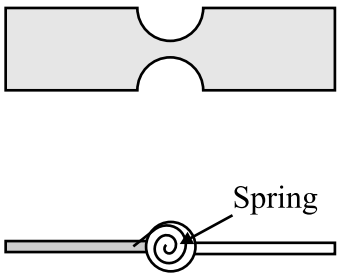

Figure 4.2: The PRBM of a circular flexure hinge

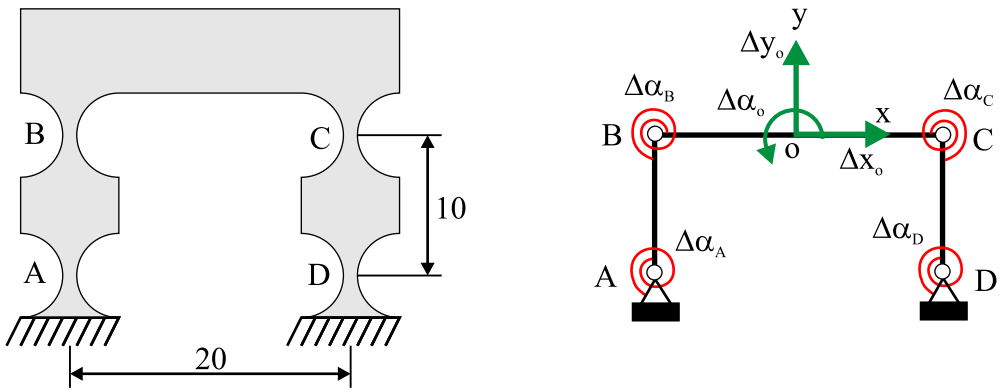

(a) Four-bar compliant mechanism

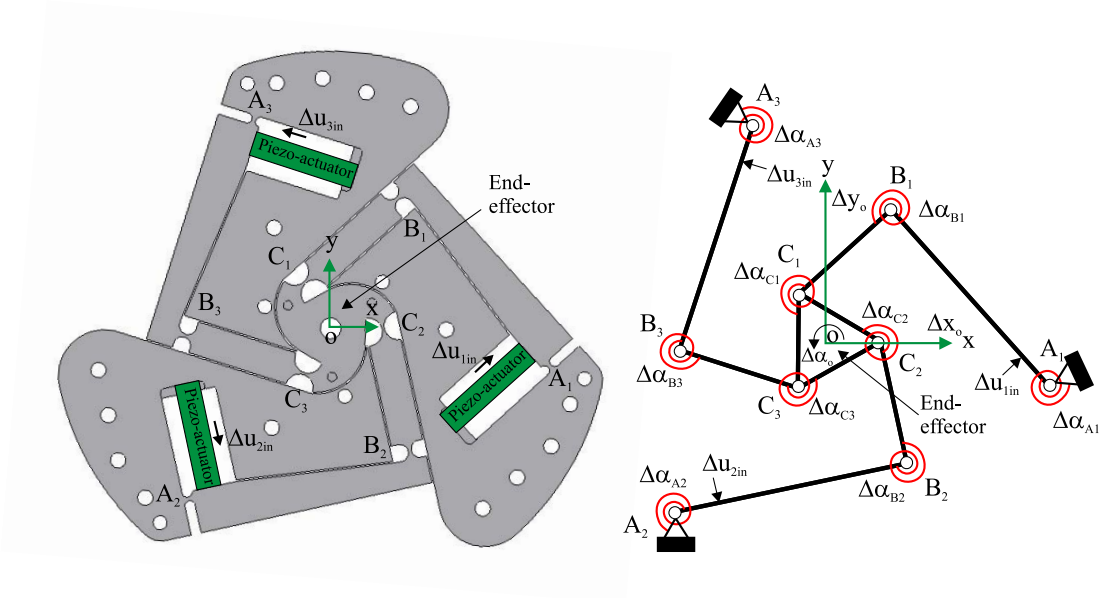

(b) 3-RRR micro-motion stage

Figure 4.3: The PRBM of micro-motion stages

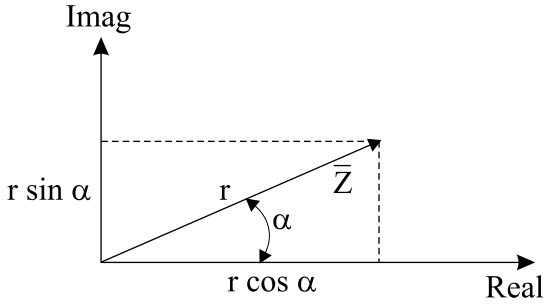

Figure 4.4: Complex plane

compliant structures. This loop equation was expressed in terms of its real and imaginary parts, resulting in two equations per loop. Unknowns were found by solving these equations simultaneously. An intensive study of this method has been carried out by Howell (2001).

Complex numbers were used to represent vectors in each closed-loop. The complex number was written as,

$$\overline{\mathbf{Z}} = re^{i\alpha} = r\left(cos\alpha + isin\alpha\right) \tag{4.1}$$

where r is the length of links, α is the initial orientations of the link as shown in Figure 4.4.

4.2 Kinematic modelling of four-bar compliant mechanisms

Flexure hinge A in Figure 4.5 is the actuated joint (active joint). Flexure hinges labelled B, C and D are unactuated (passive joints). Therefore, there are three unknowns to be solved, which are $\Delta\alpha_B$, $\Delta\alpha_C$ and $\Delta\alpha_D$. Since $\Delta\alpha_B = \Delta\alpha_C$, the number of unknowns are reduced to two which can be solved by equations obtained from a single closed-loop.

From the loop,

$$\overline{\mathbf{Z}}_{\mathbf{AB}} + \overline{\mathbf{Z}}_{\mathbf{BC}} - \overline{\mathbf{Z}}_{\mathbf{AD}} - \overline{\mathbf{Z}}_{\mathbf{DC}} = 0 \tag{4.2}$$

Loop equation obtained from the real component of Equation 4.2 is,

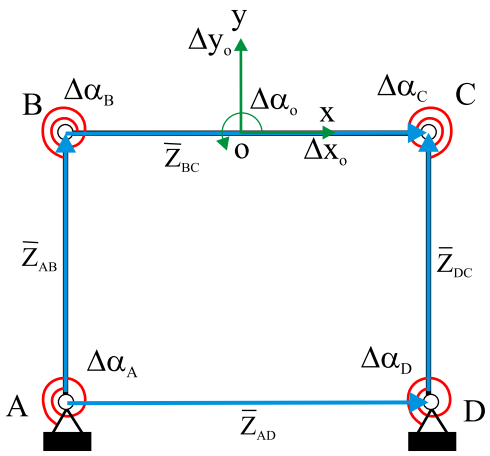

Figure 4.5: Single loop four-bar structure analysis

$$\begin{aligned} &r_{ab}cos\left(\alpha_{AB}+\Delta\alpha_A\right)+r_{bc}cos\left(\alpha_{BC}+\Delta\alpha_A+\Delta\alpha_B\right)\\ &-r_{ad}cos\left(\alpha_{AD}\right)-r_{dc}cos\left(\alpha_{DC}+\Delta\alpha_D\right)=0 \end{aligned} \tag{4.3}$$

Loop equation obtained from the imaginary component of Equation 4.2 is,

$$\begin{aligned} &r_{ab}sin\left(\alpha_{AB}+\Delta\alpha_A\right)+r_{bc}sin\left(\alpha_{BC}+\Delta\alpha_A+\Delta\alpha_B\right)\\ &-r_{ad}sin\left(\alpha_{AD}\right)-r_{dc}sin\left(\alpha_{DC}+\Delta\alpha_D\right)=0 \end{aligned} \tag{4.4}$$

where r_{ab} is the length of link A_iB_i, similarly for r_{bc}, r_{ad} and r_{dc} . α_{AB} is the argument of vector $\overline{\mathbf{Z}}_{\mathbf{AB}}$ measured from the global x-axis, similarly for α_{BC}, α_{AD} and α_{DC}.

Since the displacements are in the scale of micrometres, the small angle approximations of cosine and sine functions can be adopted, which are $cos\left(\Delta\alpha\right)\simeq 1$ and $sin\left(\Delta\alpha\right)\simeq\Delta\alpha$. By using the trigonometry identities,

$$\begin{aligned} cos\left(x\pm y\right) &= cos\,xcos\,y\mp sin\,xsin\,y\\ sin\left(x\pm y\right) &= sin\,xcos\,y\pm sin\,ycos\,x \end{aligned}$$

Equation 4.3 and 4.4 can be simplified as,

α_{AB} (rad)	α_{BC} (rad)	α_{DC} (rad)	r_{ab} (mm)	r_{bc} (mm)	r_{dc} (mm)	R_o (mm)
$\pi/2$	0	$\pi/2$	10	20	10	3.5

Table 4.1: Parameters of the PRBM of the four-bar compliant structure

$$\begin{aligned} r_{ab}\left(cos\left(\alpha_{AB}\right)-\Delta\alpha_A sin\left(\alpha_{AB}\right)\right)+r_{bc}\left(cos\left(\alpha_{BC}\right)-\left(\Delta\alpha_A+\Delta\alpha_B\right)sin\left(\alpha_{BC}\right)\right) \\ -r_{ad}cos\left(\alpha_{AD}\right)-r_{dc}\left(cos\left(\alpha_{DC}\right)-\Delta\alpha_D sin\left(\alpha_{DC}\right)\right)=0 \end{aligned} \tag{4.5}$$

$$\begin{aligned} r_{ab}\left(sin\left(\alpha_{AB}\right)+\Delta\alpha_A cos\left(\alpha_{AB}\right)\right)+r_{bc}\left(sin\left(\alpha_{BC}\right)+\left(\Delta\alpha_A+\Delta\alpha_B\right)cos\left(\alpha_{BC}\right)\right) \\ -r_{ad}sin\left(\alpha_{AD}\right)-r_{dc}\left(sin\left(\alpha_{DC}\right)+\Delta\alpha_D cos\left(\alpha_{DC}\right)\right)=0 \end{aligned} \tag{4.6}$$

and,

$$\begin{aligned} r_{ad}cos\left(\alpha_{AD}\right) &= r_{ab}cos\left(\alpha_{AB}\right)+r_{bc}cos\left(\alpha_{BC}\right)-r_{dc}cos\left(\alpha_{DC}\right) \\ r_{ad}sin\left(\alpha_{AD}\right) &= r_{ab}sin\left(\alpha_{AB}\right)+r_{bc}sin\left(\alpha_{BC}\right)-r_{dc}sin\left(\alpha_{DC}\right) \end{aligned} \tag{4.7}$$

Therefore, Equation 4.20 and 4.21 can be reduced to,

$$-r_{ab}\Delta\alpha_A sin\left(\alpha_{AB}\right)-r_{bc}\left(\Delta\alpha_A+\Delta\alpha_B\right)sin\left(\alpha_{BC}\right)+r_{dc}\Delta\alpha_D sin\left(\alpha_{DC}\right)=0 \tag{4.8}$$

$$r_{ab}\Delta\alpha_A cos\left(\alpha_{AB}\right)+r_{bc}\left(\Delta\alpha_A+\Delta\alpha_B\right)cos\left(\alpha_{BC}\right)-r_{dc}\Delta\alpha_D cos\left(\alpha_{DC}\right)=0 \tag{4.9}$$

The input angular displacements, $\Delta\alpha_A$ are,

$$\Delta\alpha_A=-\frac{\Delta u_{in}}{R_o} \tag{4.10}$$

where Δu_{in} are the input displacements caused by the piezo-actuator, R_o is the distance from the centre of the piezo-actuator to the centre of the flexure hinge as shown in Figure 4.6. The negative sign indicates that the direction of rotations are clockwise.

Table 4.1 exhibits all the parameters of the PRBM of the four-bar compliant struc-

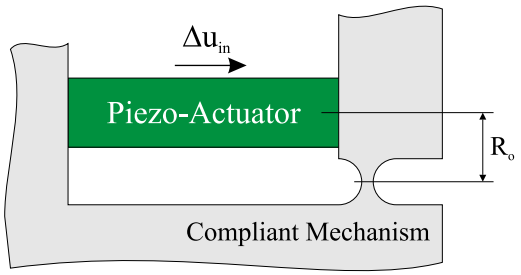

Figure 4.6: Piezo-actuator and compliant mechanism

ture. By substituting all the parameters and the input angular displacement from Equation 4.10 into Equations 4.8 and 4.9, the two equations can be solved to obtain $\Delta\alpha_B$ and $\Delta\alpha_D$. These angular displacements are expressed in terms of the input displacements of the piezo-actuator, Δu_{in},

$$\Delta\alpha_B = c_1 \Delta u_{in} \tag{4.11}$$

$$\Delta\alpha_D = c_2 \Delta u_{in} \tag{4.12}$$

where c_1 and c_2 are constants.
By determining all the unknown angular displacements of flexure hinges, the kinematics of the four-bar compliant mechanism can be derived easily to find the output displacements (Δx_o, Δy_o, $\Delta\alpha_o$) of the end-effector when the input displacements, Δu_{in} are given. A Jacobian matrix is normally used to relate the velocity of an end-effector to the velocity of actuators. However, for the case of micro-motion stages, the displacements of the piezo-actuators are substantially small compare to the link lengths and the motions of the micro-motion stages are also very small. Therefore, the micro-motion stages are almost configurationally invariant and its Jacobian matrix is assumed to be constant. The Jacobian of the four-bar compliant mechanism can be defined as a constant matrix to relate the output displacements of the end-effector ($\Delta x_o\ \Delta y_o\ \Delta\alpha_o$) to the input displacements of the piezo-actuators (Δu_{in}) as below,

$$\begin{bmatrix} \Delta x_o \\ \Delta y_o \\ \Delta\alpha_o \end{bmatrix} = \mathbf{J_{PRBM,4bar}}\ \Delta u_{in} \tag{4.13}$$

The Jacobian matrix of the four-bar compliant mechanism is calculated as below,

$$\mathbf{J_{PRBM,4bar}} = \begin{bmatrix} 2.857 \\ 0.59 \times 10^{-9} \\ 0 \end{bmatrix} \tag{4.14}$$

It is observed that the Δy_o term in Equation 4.14 is very small and can be assumed to be zero.

4.3 Kinematic modelling of 3-RRR compliant micro-motion stages

All flexure hinges labelled A_i in Figure 4.7 are actuated (active joints). Flexure hinges labelled B_i and C_i are unactuated (passive joints). Therefore, $\Delta\alpha_{B_i}$ and $\Delta\alpha_{C_i}$ (i= 1, 2, 3) are unknowns. Six equations were required to solve these six unknowns, which leads to the need of generating three loop equations. Due to the advantage of the closed-loop configuration of the 3-RRR structure, the two relationships below can be determined from the geometry of the 3-RRR structure,

$$\begin{aligned} \Delta\alpha_{A_2} + \Delta\alpha_{B_2} + \Delta\alpha_{C_2} &= \Delta\alpha_{A_1} + \Delta\alpha_{B_1} + \Delta\alpha_{C_1} \\ \Delta\alpha_{C_2} &= \Delta\alpha_{A_1} + \Delta\alpha_{B_1} + \Delta\alpha_{C_1} - \Delta\alpha_{A_2} - \Delta\alpha_{B_2} \end{aligned} \tag{4.15}$$

$$\begin{aligned} \Delta\alpha_{A_3} + \Delta\alpha_{B_3} + \Delta\alpha_{C_3} &= \Delta\alpha_{A_1} + \Delta\alpha_{B_1} + \Delta\alpha_{C_1} \\ \Delta\alpha_{C_3} &= \Delta\alpha_{A_1} + \Delta\alpha_{B_1} + \Delta\alpha_{C_1} - \Delta\alpha_{A_3} - \Delta\alpha_{B_3} \end{aligned} \tag{4.16}$$

Therefore, there are only four unknowns which required only four equations. The number of loops required is therefore reduced from three to two loops, which simplifies the modelling process of the 3-RRR mechanism.
Loop 1,

$$\overline{\mathbf{Z}}_{\mathbf{A_1B_1}} + \overline{\mathbf{Z}}_{\mathbf{B_1C_1}} + \overline{\mathbf{Z}}_{\mathbf{C_1C_3}} - \left(\overline{\mathbf{Z}}_{\mathbf{A_1A_3}} + \overline{\mathbf{Z}}_{\mathbf{A_3B_3}} + \overline{\mathbf{Z}}_{\mathbf{B_3C_3}}\right) = 0 \tag{4.17}$$

Loop equation obtained from the real component of Equation 4.17 is,

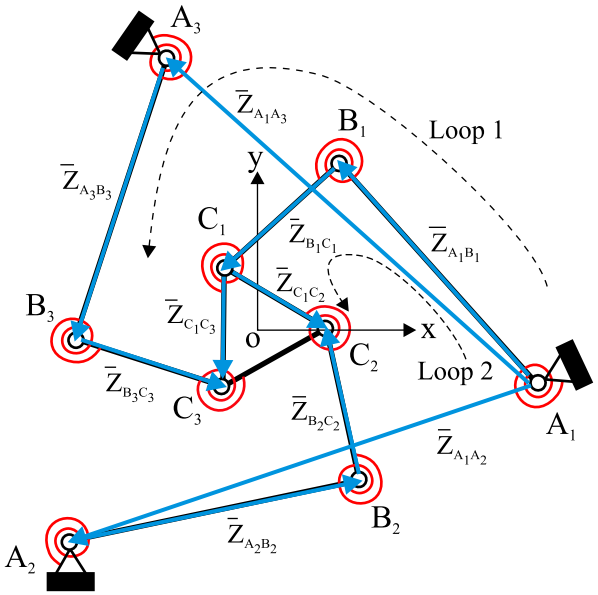

Figure 4.7: Two-loop 3-RRR structure analysis

$$
\begin{aligned}
&r_{ab}cos\left(\alpha_{A_1B_1}+\Delta\alpha_{A_1}\right)+r_{bc}cos\left(\alpha_{B_1C_1}+\Delta\alpha_{A_1}+\Delta\alpha_{B_1}\right)\\
&+r_{cc}cos\left(\alpha_{C_1C_3}+\Delta\alpha_{A_1}+\Delta\alpha_{B_1}+\Delta\alpha_{C_1}\right)\\
&-r_{aa}cos\left(\alpha_{A_1A_3}\right)-r_{ab}cos\left(\alpha_{A_3B_3}+\Delta\alpha_{A_3}\right)\\
&-r_{bc}cos\left(\alpha_{B_3C_3}+\Delta\alpha_{A_3}+\Delta\alpha_{B_3}\right)=0
\end{aligned}
\tag{4.18}
$$

Loop equation obtained from the imaginary component of Equation 4.17 is,

$$
\begin{aligned}
&r_{ab}sin\left(\alpha_{A_1B_1}+\Delta\alpha_{A_1}\right)+r_{bc}sin\left(\alpha_{B_1C_1}+\Delta\alpha_{A_1}+\Delta\alpha_{B_1}\right)\\
&+r_{cc}sin\left(\alpha_{C_1C_3}+\Delta\alpha_{A_1}+\Delta\alpha_{B_1}+\Delta\alpha_{C_1}\right)\\
&-r_{aa}sin\left(\alpha_{A_1A_3}\right)-r_{ab}sin\left(\alpha_{A_3B_3}+\Delta\alpha_{A_3}\right)\\
&-r_{bc}sin\left(\alpha_{B_3C_3}+\Delta\alpha_{A_3}+\Delta\alpha_{B_3}\right)=0
\end{aligned}
\tag{4.19}
$$

where r_{ab} is the length of link A_iB_i, r_{bc} is the length of link B_iC_i, r_{cc} is the length of link C_iC_j ($i \neq j$, i = j = 1, 2, 3), r_{aa} is the length of link A_iA_j. $\alpha_{A_1A_3}$ is the argument of vector $\overline{\mathbf{Z}}_{\mathbf{A_1A_3}}$ measured from the global x-axis, similarly for $\alpha_{A_1B_1}$, $\alpha_{B_1C_1}$, $\alpha_{C_1C_3}$, $\alpha_{A_1A_3}$, $\alpha_{A_3B_3}$ and $\alpha_{A_3C_3}$.

Since the displacements are in the scale of micrometres, the small angle approximations of cosine and sine functions can be adopted, which are $cos\left(\Delta\alpha\right) \simeq 1$ and

$sin\,(\Delta\alpha) \simeq \Delta\alpha$. By using the trigonometry identities, Equation 4.18 and 4.19 can be simplified as,

$$\begin{gathered} r_{ab}\,(cos\,(\alpha_{A_1B_1}) - \Delta\alpha_{A_1} sin\,(\alpha_{A_1B_1})) \\ +r_{bc}\,(cos\,(\alpha_{B_1C_1}) - (\Delta\alpha_{A_1} + \Delta\alpha_{B_1})\,sin\,(\alpha_{B_1C_1})) \\ +r_{cc}\,(cos\,(\alpha_{C_1C_3}) - (\Delta\alpha_{A_1} + \Delta\alpha_{B_1} + \Delta\alpha_{C_1})\,sin\,(\alpha_{C_1C_3})) \\ -r_{aa} cos\,(\alpha_{A_1A_3}) - r_{ab}\,(cos\,(\alpha_{A_3B_3}) - \Delta\alpha_{A_3} sin\,(\alpha_{A_3B_3})) \\ -r_{bc}\,(cos\,(\alpha_{B_3C_3}) - (\Delta\alpha_{A_3} + \Delta\alpha_{B_3})\,sin\,(\alpha_{B_3C_3})) = 0 \end{gathered} \tag{4.20}$$

$$\begin{gathered} r_{ab}\,(sin\,(\alpha_{A_1B_1}) + \Delta\alpha_{A_1} cos\,(\alpha_{A_1B_1})) \\ +r_{bc}\,(sin\,(\alpha_{B_1C_1}) + (\Delta\alpha_{A_1} + \Delta\alpha_{B_1})\,cos\,(\alpha_{B_1C_1})) \\ +r_{cc}\,(sin\,(\alpha_{C_1C_3}) + (\Delta\alpha_{A_1} + \Delta\alpha_{B_1} + \Delta\alpha_{C_1})\,cos\,(\alpha_{C_1C_3})) \\ -r_{aa} sin\,(\alpha_{A_1A_3}) - r_{ab}\,(sin\,(\alpha_{A_3B_3}) + \Delta\alpha_{A_3} cos\,(\alpha_{A_3B_3})) \\ -r_{bc}\,(sin\,(\alpha_{B_3C_3}) + (\Delta\alpha_{A_3} + \Delta\alpha_{B_3})\,cos\,(\alpha_{B_3C_3})) = 0 \end{gathered} \tag{4.21}$$

and,

$$\begin{aligned} r_{aa} cos\,(\alpha_{A_1A_3}) &= r_{ab} cos\,(\alpha_{A_1B_1}) + r_{bc} cos\,(\alpha_{B_1C_1}) + r_{cc} cos\,(\alpha_{C_1C_3}) \\ &\quad -r_{ab} cos\,(\alpha_{A_3B_3}) - r_{bc} cos\,(\alpha_{B_3C_3}) \\ r_{aa} sin\,(\alpha_{A_1A_3}) &= r_{ab} sin\,(\alpha_{A_1B_1}) + r_{bc} sin\,(\alpha_{B_1C_1}) + r_{cc} sin\,(\alpha_{C_1C_3}) \\ &\quad -r_{ab} sin\,(\alpha_{A_3B_3}) - r_{bc} sin\,(\alpha_{B_3C_3}) \end{aligned} \tag{4.22}$$

Therefore, Equation 4.20 and 4.21 can be reduced to,

$$\begin{gathered} -r_{ab}\Delta\alpha_{A_1} sin\,(\alpha_{A_1B_1}) - r_{bc}\,(\Delta\alpha_{A_1} + \Delta\alpha_{B_1})\,sin\,(\alpha_{B_1C_1}) \\ -r_{cc}\,(\Delta\alpha_{A_1} + \Delta\alpha_{B_1} + \Delta\alpha_{C_1})\,sin\,(\alpha_{C_1C_3}) \\ +r_{ab}\Delta\alpha_{A_3} sin\,(\alpha_{A_3C_3}) + r_{bc}\,(\Delta\alpha_{A_3} + \Delta\alpha_{B_3})\,sin\,(\alpha_{B_3C_3}) = 0 \end{gathered} \tag{4.23}$$

$$\begin{gathered} r_{ab}\Delta\alpha_{A_1} cos\,(\alpha_{A_1B_1}) + r_{bc}\,(\Delta\alpha_{A_1} + \Delta\alpha_{B_1})\,cos\,(\alpha_{B_1C_1}) \\ +r_{cc}\,(\Delta\alpha_{A_1} + \Delta\alpha_{B_1} + \Delta\alpha_{C_1})\,cos\,(\alpha_{C_1C_3}) \\ -r_{ab}\Delta\alpha_{A_3} cos\,(\alpha_{A_3C_3}) - r_{bc}\,(\Delta\alpha_{A_3} + \Delta\alpha_{B_3})\,cos\,(\alpha_{B_3C_3}) = 0 \end{gathered} \tag{4.24}$$

Similarly for loop 2,

$$\overline{\mathbf{Z}}_{\mathbf{A_1B_1}} + \overline{\mathbf{Z}}_{\mathbf{B_1C_1}} + \overline{\mathbf{Z}}_{\mathbf{C_1C_2}} - \left(\overline{\mathbf{Z}}_{\mathbf{A_1A_2}} + \overline{\mathbf{Z}}_{\mathbf{A_2B_2}} + \overline{\mathbf{Z}}_{\mathbf{B_2C_2}}\right) = 0 \tag{4.25}$$

Loop equations obtained from Equation 4.25 are,

$$\begin{aligned} &-r_{ab}\Delta\alpha_{A_1} sin\left(\alpha_{A_1B_1}\right) - r_{bc}\left(\Delta\alpha_{A_1} + \Delta\alpha_{B_1}\right) sin\left(\alpha_{B_1C_1}\right) \\ &-r_{cc}\left(\Delta\alpha_{A_1} + \Delta\alpha_{B_1} + \Delta\alpha_{C_1}\right) sin\left(\alpha_{C_1C_2}\right) \\ &+r_{ab}\Delta\alpha_{A_2} sin\left(\alpha_{A_2B_2}\right) + r_{bc}\left(\Delta\alpha_{A_2} + \Delta\alpha_{B_2}\right) sin\left(\alpha_{B_2C_2}\right) = 0 \end{aligned} \tag{4.26}$$

$$\begin{aligned} &r_{ab}\Delta\alpha_{A_1} cos\left(\alpha_{A_1B_1}\right) + r_{bc}\left(\Delta\alpha_{A_1} + \Delta\alpha_{B_1}\right) cos\left(\alpha_{B_1C_1}\right) \\ &+r_{cc}\left(\Delta\alpha_{A_1} + \Delta\alpha_{B_1} + \Delta\alpha_{C_1}\right) cos\left(\alpha_{C_1C_2}\right) \\ &-r_{ab}\Delta\alpha_{A_2} cos\left(\alpha_{A_2B_2}\right) - r_{bc}\left(\Delta\alpha_{A_2} + \Delta\alpha_{B_2}\right) cos\left(\alpha_{B_2C_2}\right) = 0 \end{aligned} \tag{4.27}$$

The three input angular displacements, $\Delta\alpha_{A_i}$ (i=1, 2, 3) are,

$$\Delta\alpha_{A_i} = -\frac{\Delta u_{kin}}{R_o} \tag{4.28}$$

where Δu_{kin} (k = 1, 2, 3) are the input displacements caused by the three piezo-actuators respectively, R_o is the distance shown in Figure 4.6. The negative sign indicates that the direction of rotation is clockwise.

Table 4.2 exhibits all the parameters of the PRBM of the 3-RRR micro-motion stage. By substituting all the parameters and the three input angular displacements from Equation 4.28 into Equations 4.23, 4.24, 4.26 and 4.27, they can be solved together with Equations 4.15 and 4.16 to obtain all the unknown angular displacements, $\Delta\alpha_{B_i}$ and $\Delta\alpha_{C_i}$. These angular displacements are expressed in terms of the input displacements of the three piezo-actuators, Δu_{kin}.

$$\begin{bmatrix} \Delta\alpha_{B_1} \\ \Delta\alpha_{B_2} \\ \Delta\alpha_{B_3} \end{bmatrix} = \Omega_B \begin{bmatrix} \Delta u_{1in} \\ \Delta u_{2in} \\ \Delta u_{3in} \end{bmatrix} \tag{4.29}$$

	$i = 1$	$i = 2$	$i = 3$
$\alpha_{A_iB_i}$ (rad)	2.391	0.297	-1.798
$\alpha_{B_iC_i}$ (rad)	-2.321	1.867	-0.227

$\alpha_{C_1C_2}$ (rad)	-0.452
$\alpha_{C_1C_3}$ (rad)	-1.450
r_{ab} (mm)	49.0
r_{bc} (mm)	27.0
r_{cc} (mm)	19.7
R_o (mm)	5.1

Table 4.2: Parameters of the PRBM of the 3-RRR micro-motion stage

$$\begin{bmatrix} \Delta\alpha_{C_1} \\ \Delta\alpha_{C_2} \\ \Delta\alpha_{C_3} \end{bmatrix} = \Omega_C \begin{bmatrix} \Delta u_{1in} \\ \Delta u_{2in} \\ \Delta u_{3in} \end{bmatrix} \tag{4.30}$$

where Ω_B and Ω_C are 3x3 matrices.

By knowing all the unknown angular displacements of flexure hinges, the kinematics of the micro-motion stage can be derived easily to find the output displacements and orientations (Δx_o, Δy_o, $\Delta\alpha_o$) of the end-effector when the input displacements (Δu_{1in}, Δu_{2in}, Δu_{3in}) are given. Since the 3-RRR compliant micro-motion stage is almost configurationally invariant (as explained in Section 4.2), a constant Jacobian matrix can be derived to relate the input displacements to the output displacements as below,

$$\begin{bmatrix} \Delta x_o \\ \Delta y_o \\ \Delta\alpha_o \end{bmatrix} = \mathbf{J_{PRBM,3RRR}} \begin{bmatrix} \Delta u_{1in} \\ \Delta u_{2in} \\ \Delta u_{3in} \end{bmatrix} \tag{4.31}$$

The Jacobian matrix of the PRBM is calculated as below,

$$\mathbf{J_{PRBM,3RRR}} = \begin{bmatrix} 4.37 & 1.87 & -6.24 \\ 4.68 & -6.12 & 1.44 \\ -288.73 & -288.73 & -288.73 \end{bmatrix} \tag{4.32}$$

4.4 Concluding remarks

The PRBM method that models flexure hinges to have only one-DOF may introduce some inaccuracies in the kinematic model. In order to compare the modelling accuracy of the PRBM method to the kinetostatic model developed in this thesis, the kinematic models of a four-bar compliant mechanism and a 3-RRR micromotion stage were derived using the loop-closure theory and the PRBM method. The loop-closure theory incorporates the complex number method to model the kinematics of mechanisms. A loop equation was generated for each closed-loop in the compliant structures. These loop equation were expressed in terms of its real and imaginary parts, resulting in two equations per loop. Unknowns were found by solving these equations simultaneously. Since the displacements were in micro-scale, the small angle approximations of cosine and sine functions can be adopted to simplify the modelling process. The kinematic results derived using the PRBM method and the loop-closure theory in this chapter will be compared to the kinetostatic model, FEA and experimental results presented in Chapters 5, 6 and 7 respectively. The results of these comparisons will highlight the advantage of the kinetostatic model.